Neural Computing and Applications (2024) 36:18781–18805
https://doi.org/10.1007/s00521-024-10189-z

ORIGINAL ARTICLE

Early-stage stroke prediction based on Parkinson and wrinkles using deep learning

T. Haritha[1] · A. V. Santhosh Babu[2]

Received: 20 October 2023 / Accepted: 5 July 2024 / Published online: 31 July 2024
© The Author(s), under exclusive licence to Springer-Verlag London Ltd., part of Springer Nature 2024

Abstract
The application of noninvasive methods to enhance healthcare systems has been facilitated by the development of new technology. Among the four major cardiovascular diseases, stroke is one of the deadliest and potentially fatal, but, if detected early enough, a patient's life may be spared. Most stroke research has centered on MRI and CT scans for uncomplicated categorization. This medical approach (imaging) is costly, time-consuming and needs the utilization of complex technology. To make up for these shortcomings, however, there has been a lot of interest in adopting noninvasive, measurable EEGs. Nevertheless, the raw data should be classified before the proper characteristics can be formed, both the forecasting algorithms and the analytical techniques demand time. As a result, this work proposes a deep learning-based model that aims to predict the chance of stroke at an early stage utilizing Parkinson's disease and wrinkles as markers. A patient may have a stroke disease if they are diagnosed with both Parkinson's disease and wrinkles. To the best of our knowledge, this research is the first to use these biomarkers to predict the risk of having a stroke. The proposed model achieves a higher accuracy of 94.7% on the considered dataset. Additionally, the recommended model was evaluated and tested in terms of loss, training time, accuracy, recall, and F1-score versus the other existing models. With less price and pain than present testing approaches, these discoveries are predicted to result in major enhancements in the early detection of strokes.

Keywords Stroke prediction · Stroke disease analysis · Classification · Parkinson · Deep learning

1 Introduction

A stroke is a condition that is characterized by abnormalities in the blood arteries of the brain, which leads to dysfunction in particular regions of the brain. The World Health Organization (WHO) reports that stroke is now the second most prevalent cause of death worldwide and the third leading cause of disability [1]. Patients who have had strokes are more likely to suffer from complex and varied chronic repercussions, such as cerebral edema, pneumonia, and heart failure, in addition to vascular embolism, which places a significant demand on the available medical resources. The earlier a diagnosis is made, the better the functional results and the more effectively it can prevent strokes [2].

Even though there is currently no specific cure for strokes in the realm of medical research, prompt identification is essential for the management of strokes. A timely diagnosis can help prevent disabilities, fatalities, and other major brain-related disorders [3]. Both magnetic resonance imaging (MRI) and computed tomography are used in the vast bulk of the stroke detection research that is being conducted today (CT). In any case, though, people are put in danger of being exposed to radiation, which can bring on allergic responses. In addition, computed tomography (CT) and magnetic resonance imaging (MRI) scans are highly expensive methods of diagnosis; hence, people living in

✉ T. Haritha
haritha@vcew.ac.in

A. V. Santhosh Babu
santhoshbabu@vcew.ac.in

[1] Department of Information Technology, Vivekanandha College of Engineering for Women, Tiruchengode, Tamilnadu, India

[2] Department of Computer Science and Engineering, Vivekanandha College of Engineering for Women, Tiruchengode, Tamilnadu, India

impoverished countries are unable to afford to employ these procedures [4–7]. Noninvasive methods, such as the electroencephalogram (EEG), are gaining popularity as a cost-effective or low-cost alternative to traditional diagnostic procedures [1, 8].

A software-based method for diagnosing depression is also being developed as part of the research that was published in [9]. This technique distinguishes between aberrant brain signals that could cause strokes and normal brain signals using deep learning and EEG readings. The authors [10] developed a single mechanism that can detect strokes in addition to measuring time and length. Even though it has only a 73.8% accuracy rate, the EEG and galvanic skin response (GSR) data were merged by the researchers of the paper [11] to identify strokes. The authors of [8] used bioelectrical data with natural language processing to create their research. After that, machine learning was utilized to differentiate between normal and stroke-related data.

A bidirectional Deep Neural Network is utilized in [12] to classify EEG-based pictures. To differentiate between the left and right hemispheres of the brain, the data from the signals are evaluated in several different parts of the brain. At some point, the signals are evaluated and categorized as abnormal or normal. The researchers have proposed a few different approaches [13–15] for treating patients who have suffered strokes to reduce the amount of damage done to brain tissue. Current treatments have several limitations, including the complexity of time and space required to provide findings, the use of expensive data collection methods such as MRI and CT scans, and the difficulty of differentiating between a real stroke and a ministroke (also known as a TIA). The prediction of strokes through the use of image processing has been the focus of several studies [2, 16–19]. The electrocardiogram (ECG) has been utilized in several studies to predict and prevent stroke problems caused by atrial fibrillation, which is a significant leading source of stroke [20–22].

According to the American Heart Association [23], the seven most important health factors and behaviors that contribute to the growing risks of heart attack and stroke are a poor diet, being overweight, having high levels of cholesterol, smoking cigarettes, having uncontrolled blood pressure, having high blood sugar, and not being physically active. Due to cerebrovascular abnormalities, diabetic patients have a 2–6 times increased risk of having a stroke. Because of this, the risk is greater in younger persons, those who have hypertension, and those who suffer from difficulties with a variety of other vascular beds. In addition to this, people who suffer from diabetes, hyperglycemia, and acute ischemic stroke have a reduced chance of responding favorably to the only treatment that is approved by the FDA, which is intravenous tissue plasminogen activator [24]. These people have a much higher risk of dying or becoming severely disabled, and they also have a lower chance of responding favorably to the treatment.

Studies have indicated a connection between Parkinson's disease (PD) and stroke, although the precise nature remains uncertain. Aging is a common factor for both PD and stroke, potentially leading to shared risk elements. Individuals with PD might face an escalated risk of ischemic stroke, potentially linked to factors like hyperhomocysteinemia. Yet, the exact mechanisms intertwining these conditions remain unclear. Understanding whether PD contributes to an increased stroke risk or if stroke heightens the likelihood of PD development is crucial. Further research is needed to untangle the relationship between these conditions, unveiling shared pathways. This exploration could pave the way for potential preventive measures and targeted treatments [53, 54].

Even though the currently published studies offer the greatest results in stroke prediction, none of them focus on predicting stroke disease based on both Parkinson's and wrinkles. This is even though the now-published works give the best results. The aim of each of these investigations is to develop a method for predicting strokes by making use of EEG and ECG data, in addition to CT and MRI images as input. Also, some of these are predicated on the correlation between having a stroke and having heart disease or diabetes. The primary objective of this research is to develop a method for estimating the likelihood of a patient suffering from Parkinson's disease and wrinkles having a stroke.

Parkinson's disease is thought to be a neurological disorder that impairs a person's capacity for motor coordination [25]. The loss of dopamine-producing neurons in the substantia nigra is the cause of this disturbance. Although the course of Parkinson's disease cannot be stopped or reversed with the drugs that are now available, certain symptomatic therapies can help with motor and non-motor difficulties. Parkinson's disease is notoriously hard to diagnose, and it is common to mix it with other neurological conditions [26]. In addition to clinical testing, computer-assisted methods that make use of empirical tests are increasingly being utilized for prompt detection of Parkinson's disease. There has been a recent uptick in the number of studies that look at handwriting and speech patterns as potential indicators of Parkinson's disease [27–29].

Handwriting data from individuals with Parkinson's illness was collected by Pereira et al. [30] using a smart pen that has been equipped with many sensors capable of recording a wide range of data. To investigate the data, they utilized deep learning technology. Rios-Urrego et al. [31] found the kinematic aspects that are most beneficial

for identifying people who have Parkinson's disease by collecting three separate feature sets from spiral drawings. These feature sets were used to identify the subjects. Naseer et al. [29] made use of a handwriting dataset and followed it up with a data augmentation method. This allowed them to attain accuracies of more than 0.90 when fourfold cross-validation was used. Impedovo et al. [32] did an in-depth analysis of the research by utilizing handwriting analysis as a method for diagnosing neurological conditions such as Parkinson's disease and Alzheimer's disease. Both of these conditions affect the nervous system. In this study, participants with Parkinson's disease underwent an evaluation of the static spiral test, often known as the SST.

Wrinkles on the face are considered a facial trait that develops as a person ages [33]. During the last several decades, numerous techniques for identifying facial wrinkles have been developed [34, 35]. The article [36] provides a comprehensive summary of the research that has been done on benchmark datasets, automatic wrinkle identification algorithms, and facial inpainting approaches. The authors of [37] devised a stroke analysis approach that is based on artificial intelligence (AI) that can detect early-stage strokes in the elderly by analyzing facial muscle abnormalities. This was accomplished by analyzing the patient's face. As a biomarker for distinguishing dementia from other forms of cognitive impairment, a patient's facial characteristics [38] are evaluated.

This work set the door for future research to be conducted utilizing Xception to build a face biomarker for the identification of dementia. It is possible to tell the faces of people who appear to have moderate dementia apart from the faces of people who do not have dementia using this method. The studies that were described before showed that the characteristics of the face may be utilized as an indication to forecast the likelihood of sickness. So, the purpose of this study is to determine whether or not a person has had a stroke by analyzing facial wrinkles. Deep learning strategies have lately been shown to perform better than traditional machine learning methods in a broad variety of scientific fields, including chemistry, physics, biology, and materials science [39]. As a consequence of this, the researchers in this work employ deep learning to forecast the sickness caused by biomarkers (Parkinson's and wrinkles).

The work's contributions are summarized as,

- To propose deep learning-based models to predict the probability of stroke disease using Parkinson's disease and wrinkles as biomarkers.
- In the first stage, Parkinson's disease is predicted for patients using DenseNet-201, and then wrinkles/non-wrinkles are classified using VGG-16 and LSTM in the second stage. If this patient suffers from Parkinson's disease and wrinkles, a stroke is feasible which is predicted in the next stage.
- This is, as far as we know, the first study to use deep learning models using wrinkles and Parkinson's disease to predict stroke risk. The suggested model has an improved overall accuracy (F1-score) in comparison with other current models.

2 Materials and methods

The proposed method for predicting the probability of stroke is included in the following section in detail.

2.1 Method outline

Below is a summary of the models that have been suggested. The models' classification accuracy has been increased when the DL techniques are being used. An overview of the models that have been proposed for predicting stroke in patients is shown in Fig. 1. There are three distinct modules in the recommended approach. With Parkinson's disease and wrinkles, this study attempts to forecast the risk of stroke.

A collection of photographs depicting Archimedean spirals serves as the foundation for the first module, which is followed by the pre-processing and addition of data. The datasets that were employed in this work were divided into three parts: the training set, the test and validation set, and the evaluation set. The DenseNet-201 is utilized to determine whether or not the spiral pictures are indicative of Parkinson's disease. The second part of the procedure begins by collecting face photos of the same patient. These images are then pre-processed, and VGG-16 is used to extract the patient's characteristics. At last, patients are divided into two categories: those with and those without wrinkles. Following the completion of the first two stages of categorization, a condition is verified to see whether or not a patient is experiencing Parkinson's disease and wrinkles. A patient is evaluated for the probability of having a stroke in the third module if it turns out that both of the conditions match turned out to be true. The dataset is created by first taking the first two modules and exporting their text characteristics as a.csv file. After that, the data are pre-processed, and an XGBoost model is utilized to provide a prediction regarding the likelihood of a stroke occurring. In the last step, the results that were anticipated are assessed using a variety of measures.

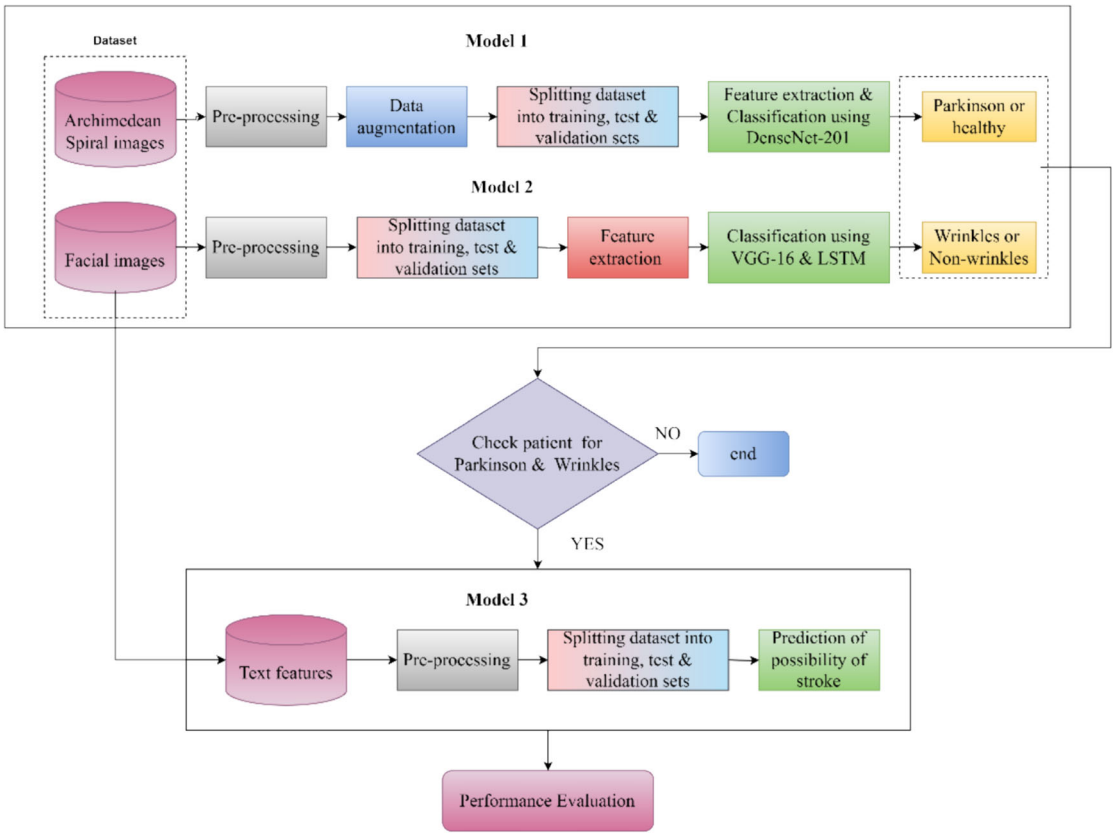


Fig. 1 Overview of the work

2.2 Dataset

The archive contains material gleaned from one hundred and two distinct people (51 patients with Parkinson's and 51 healthy). The Static Spiral Test was performed by persons utilizing a pen and paper, and the images that make up the dataset are camera-captured photographs of the hand-drawn Archimedean spirals that were obtained from these participants for the detection of Parkinson's disease. These individuals carried out the Static Spiral Test. Everyone who took part in the activity was tasked with conceptualizing their Archimedean spiral pentagon and then recreating the model that was provided. The data are to be made out in a manner that complies with the instructions, and in a manner that is both as accurate and as promptly as is practicable. Also, the data were collected from the same 102 patients who ranged in age from 18 to 80 under settings of natural light for the detection of wrinkles or non-wrinkles of a patient. It was captured in a variety of environments utilizing just the available natural light. The dataset had 102 photographs divided into the categories of wrinkled and non-wrinkled (51 patients with wrinkles and 51 non-wrinkles). In addition, a questionnaire containing personal information, such as smoking status, as well as a consent form is distributed to participants to obtain their permission to make use of their photographs in research activities. The images were captured with a Canon EOS 600D and a flash that was turned on during the process. The Parkinson and wrinkle dataset used in this work is split into a training dataset that makes up 70% of the total and a test dataset that makes up the remaining 30%. After applying data augmentation techniques, the sizes of both the spiral image dataset and the wrinkles/non-wrinkle image dataset have been increased to 360 images each.

2.2.1 Data pre-processing of static spiral test's spiral images

Pattern recognition and machine learning are both procedures that rely heavily on pre-processing to ensure accurate results. Binarization, image enhancement, normalization, data augmentation or noise reduction, sampling, transformation, and a variety of other procedures are among the key techniques that are utilized during the pre-processing stage and are applied to raw data. During this stage, raw data is processed in its most basic form. As CNN gets its functionality from raw data, it is essential to get rid of variations and noisy structures before starting the training process.

The image-based dataset (images obtained using the Static Spiral Test) was produced by defining the time series of each topic as picture dimensions and then correlating the coordinates of the path taken by the pen. The creation of the image-based dataset was carried out while all unfinished drawings were thrown away and destroyed. The handwritten text contains a sizeable quantity of irrelevant information that may cause the diagnosis to be inaccurate. After the removal of the uninteresting white space that was present around the image's borders, these pictures have been enlarged in addition to having their normalization completed and have then gone through the process of having their exposure levels normalized. Following that, the dataset was prepared acceptably so that it could be used as an input to a model. This was done to make the dataset usable. Following that, more photographs have been created utilizing a variety of photo enhancement methods to make the final output. Figure 2 represents static spiral images from the Static Spiral test.

Data Augmentation: The technique for augmenting entails modifying previously captured photos to generate fresh versions of them. While being trained, deep neural networks often require a substantial quantity of data. Even when transfer learning is utilized, training benefits from having a larger number of samples to work with. Because differences in orientation and contrast do not directly alter picture class or even the general perceptual task associated with the Static Spiral Test, the dataset has had the following data augmentations done to it.

- There is a 50% possibility that the picture will be flipped horizontally after a random operation is performed on it.
- There is a 0.1% possibility that the image's contrast will be adjusted randomly.
- There is a one in three possibility that the image may undergo a random zooming in and cropping when it is processed.

2.2.2 Pre-processing of wrinkle/ non-wrinkle images

The dataset contains photographs of varied widths, heights, as well as sizes; nevertheless, to attain consistency, all of the images were scaled to 240 pixels by 240 pixels. Image Enhancement appears to be an essential strategy for improving the overall visual appearance of a picture; it is described as the process of producing a "better" transformation form for future automated diagnostic operations.

By limiting the amplification, contrast-limited adaptive histogram equalization, or CLAHE for short, is one type of adaptive histogram equalization that can get around this problem. CLAHE is utilized almost exclusively to prevent the amplification of noise. CLAHE is an upgraded version of AHE, which stands for Adaptive Histogram Classification and is widely acknowledged to be the most effective pre-processing enhancement strategy available. Face identification is accomplished with the help of the Face + + detector, which may be accessed by the general public. After that, the picture that has been pre-processed is sent through the pre-trained network to have its features extracted. Afterward, the retrieved data characteristics were fed into the LSTM classifier so that classification could be performed on them. Figure 3 is a representation of the sample wrinkle and non-wrinkle photographs from the dataset after CLAHE and Face + + techniques.

2.3 Module 1: detection of Parkinson's disease

This section describes the detection and classification of Parkinson's disease using the DenseNet Model.

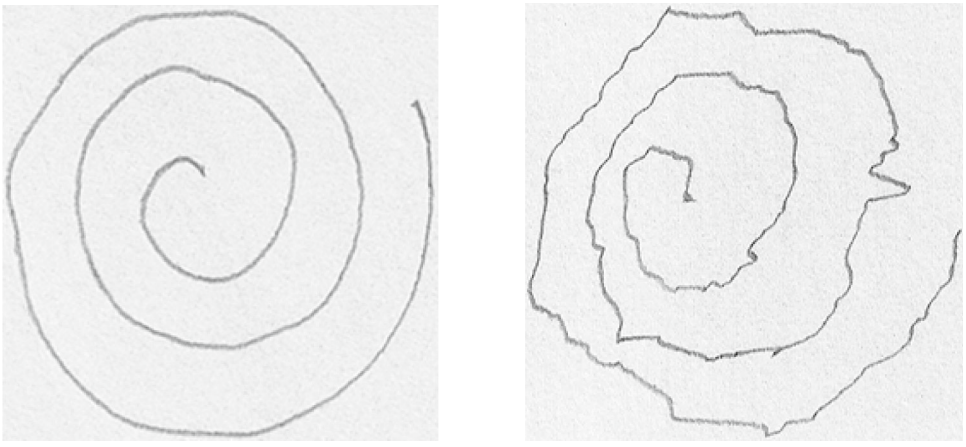


Fig. 2 Static Spiral test's Spiral samples **a** Healthy **b** Parkinson

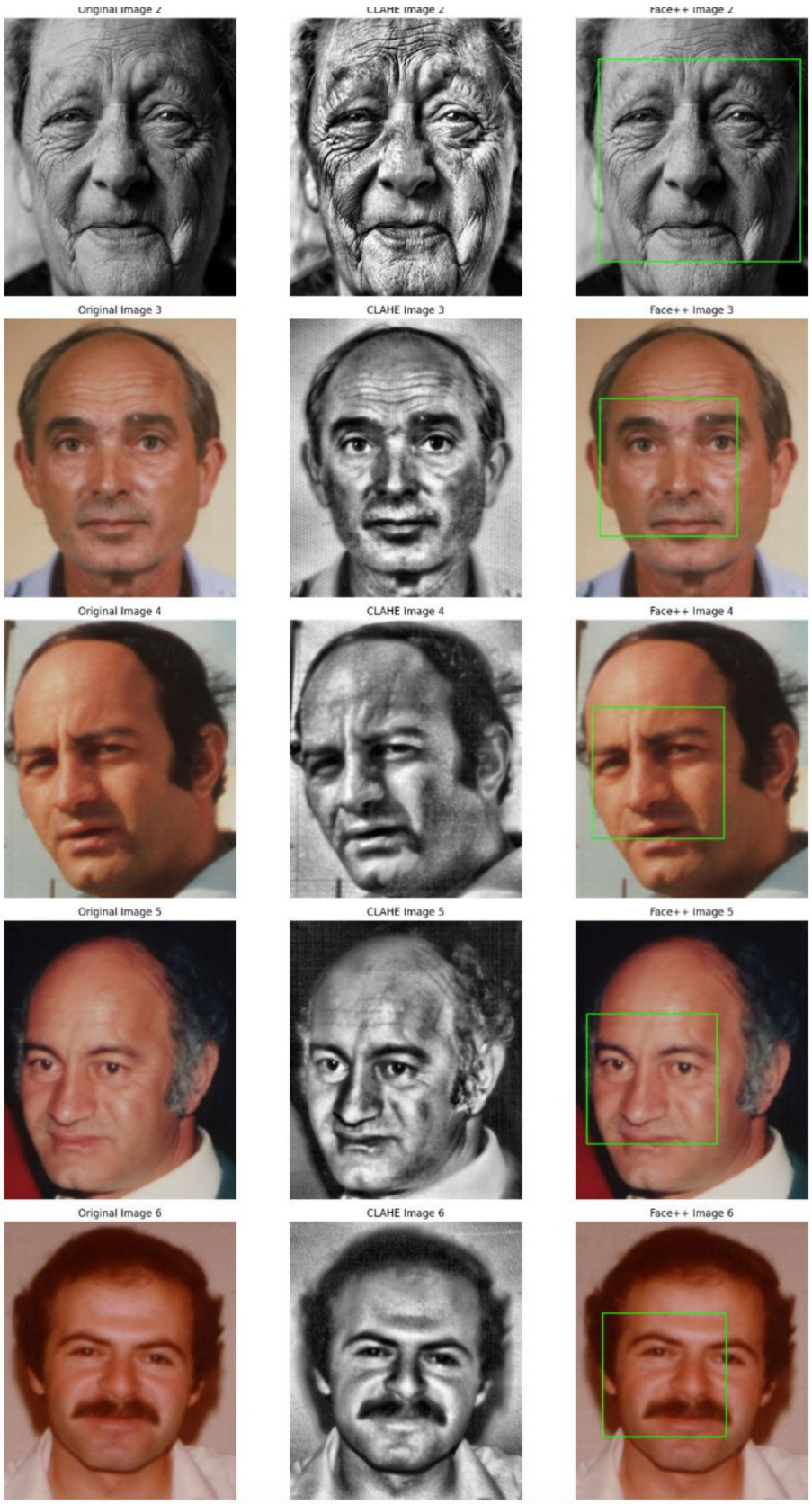


Fig. 3 Wrinkle/Non-Wrinkle data samples after CLAHE and FACE + + techniques

2.3.1 Deep transfer learning-based Parkinson's disease classification

The standard CNN primer may be found in [40]. Nevertheless, the network may have difficulty expanding both vertically and horizontally in a traditional CNN because of the possible explosion or gradient vanishing issue resulting from the progressive linking of all layers as in Eq. (1). DenseNet is a newer CNN structure for visual object identification as it outperforms well with minimum parameters. DenseNet and ResNet are very similar despite some major differences. ResNet uses an extra attribute (+) to integrate the preceding layer with the succeeding layers, whereas DenseNet just uses concatenated (.) characteristics, as shown in Eq. (1). (2). The problem is intended to be fixed by the DenseNet Architecture, which heavily interconnects all layers. DenseNet [41] merged all the feature maps from the preceding levels into one, indicating that nearly all feature maps are sent to the next layer and connected to freshly generated feature maps.

$$X_N = H_N(X_{N-1}) + X_{N-1} \tag{1}$$

$$X_N = H_N[\text{concat}(X_0, X_1, X_2, \ldots . X_{N-1})] \tag{2}$$

$$X_N = H_N(X_{N-1}) \tag{3}$$

In the equations that have been presented thus far, the layer index N and the feature that is present in the Nth layer are denoted by the symbols N and X N, respectively. Moreover, the letter H denotes a non-linear operation. Because DenseNet-201 performed the best when used for the ImageNet classification challenge, it was selected for the classification of Parkinson's disease in this study. The recently developed version of DenseNet has several benefits, one of which is feature reuse, which helps to mitigate the problems of exploding and gradient vanishing [42]. The fundamental principles of transfer learning involve employing a sophisticated and effective pre-trained model, specifically DenseNet in this work. This model is trained first on a large-scale dataset, like ImageNet, and then "transfers" the learned information to a relatively easier task that is, identifying Parkinson's disease from healthy individuals even with sparse data. The original pre-trained DenseNet-201 consists of a Fully Connected Layer (FCL) of 1000 nodes with pre-trained weights and biases. In the Modified DenseNet-201, this layer is substituted with a new FCL comprising only 2 nodes, initialized randomly. The initial DenseNet-201 model's Classification Layer encompassed 1000 diverse classes such as a recreational vehicle, printer, coho, milk can, Irish wolfhound, and numerous others, alongside 980 additional classes. However, in the Modified DenseNet-201, this classification layer is adapted to accommodate just two classes: Parkinson's and healthy.

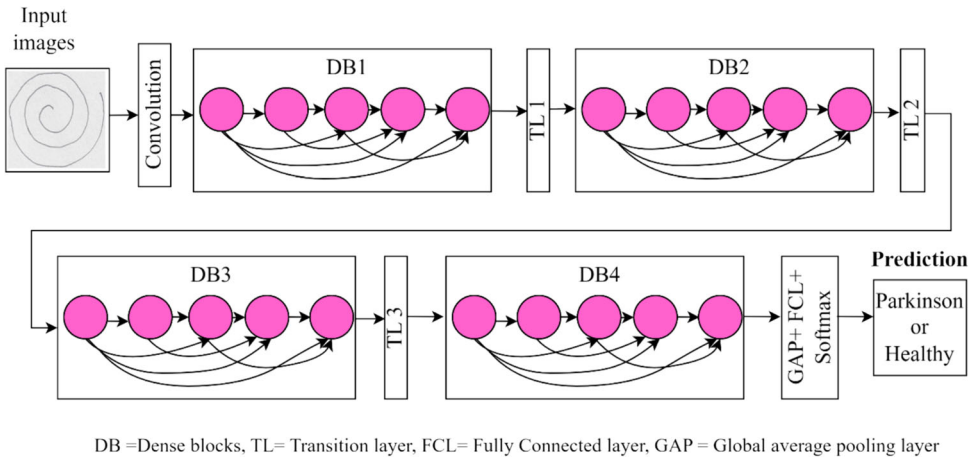
In addition, the following adjustments need to be made to make the DenseNet architecture effective. One of these adjustments involves down-sampling the feature maps to make concatenation possible. Because of the varying sizes of the feature maps, completing the concatenation process might be difficult. After that, the idea of thick blocks was developed as a means of putting down-sampling into practice. As seen in Fig. 4, transition layers may be found in the spaces in between dense blocks. These layers are made up of the processes of batch normalization, convolution, and pooling. It is important to note that the network receives a considerable number of inputs; hence, a bottleneck layer was included in the DenseNet to minimize feature maps and cut down on the expenses of computation. This is done by placing a 1×1 convolution layer in front of a 3×3 convolution layer. This sequence of layers is called a convolution chain. DenseBlocks were suggested to be implemented by utilizing transition layers (TLs). Using TL can primarily result in two advantageous outcomes: I This may result in a decrease in the number of feature maps: assume a DenseBlock creates k feature maps with a compression factor of between 0 and 1. After that, the NFM of the feature maps is going to be lowered to l. If the value is equal to 1, the feature maps will remain unchanged.

$$H_{fm} = \begin{cases} l \text{ before TL} \\ \theta \times l \text{after TL} \end{cases} \tag{4}$$

(ii) TL layers are another option for achieving the desired down-sampling effect. It is possible to do this by performing a 1×1 convolution followed by a 2×2 pooling operation in the space that separates two consecutive dense blocks. In addition to this, the feature maps are concatenated since the size of the feature maps is consistent throughout all dense blocks.

The construction of DenseNet is shown in Fig. 5. It consists of four databases (DBs), an input layer, transition layers (TLs), and a gap layer. The TLs are built with the following layers: batch normalization, convolution with a size of one by one, and an average pooling layer with a size of two by two and a stride of two. The TLs consist of a batch normalization layer, a 1×1 convolution layer, and a 2×2 average pooling layer with a stride of 2 in each of their layers. The GAP approach succeeds in accomplishing a more significant decrease in feature size, going from ggc to 1c. It is analogous to the standard Maximum Pooling (MP) and Average Pooling (AP) processes that are often used. As a direct consequence of the GAP layer, the overall thickness of the slice is reduced to a single digit.

$$SI_{fm} = \begin{cases} g \times g \times c \, before \, GAP \\ 1 \times 1 \times c \, after \, GAP \end{cases} \tag{5}$$



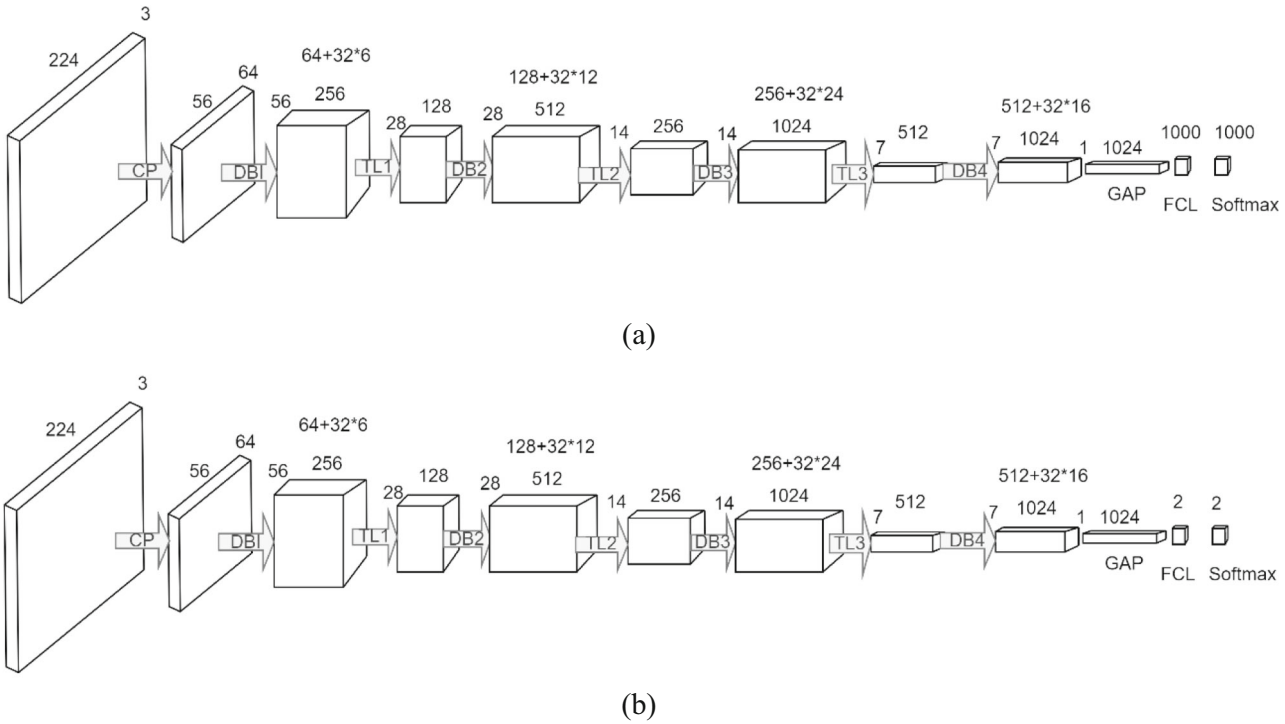


Fig. 4 Spiral image classification using the DenseNet-201 model

Fig. 5 Architecture of **a** Original pre-trained DenseNet-201 **b** Modified DenseNet-201

The structure of the model has been modified in some way. Although the initial completely connected layer (FCL) was developed to recognize 1000 categories, the final dense layer, which is also known as a fully connected layer (FCL), has been modified. A few examples of different classes include the zebra, the miniskirt, the pencil box, and the rocking rocker. Yet, none of them are connected to Parkinson's disease, which serves as the principal example of a classification challenge in this investigation. Considering that the number of output neurons in a typical DenseNet (length = 1000) is not comparable to the number of classifications in this study (which is 2, as shown in Fig. 5), the conclusion is that the conventional DenseNet is not optimal (b). Hence, just two neurons are used to make adjustments to both the final FCL and the classification layer. The Parkinson and healthy classes will be the final output from the model after it has been categorized. The breakdown of the proposed DenseNet-201 model is shown in Table 1.

2.4 Module 2: detection of wrinkles

The identification and categorization of wrinkles using a pre-trained VGG-16 and LSTM model is covered in this

Table 1 The proposed DenseNet-201 model's summary

Layer (type)	Output shape	Parameters
Convolution	1, 64, 112, 112	9408
Pooling	1, 64, 56, 56	0
Dense block 1	1, 256, 56, 56	335040
Transition layer 1	1, 128, 28, 28	33280
Dense block 2	1, 512, 28, 28	919680
Transition layer 2	1, 256, 14, 14	132096
Dense block 3	1, 1792, 14, 14	8071680
Transition layer 3	1, 896, 7, 7	1609216
Dense block 4	1, 1920, 7, 7	6978560
Global average Pooling	1, 1920, 1, 1	0
Fully connected layer (2), softmax	1, 512	983552

section. Images of wrinkles on the forehead are examined in this research to determine the presence of wrinkles.

2.4.1 Deep transfer learning-based wrinkles disease classification

In face-based analysis, wrinkles are a very important feature. As the majority of wrinkles of interest appear in a horizontal orientation, the region of the forehead was chosen for this experiment to identify wrinkles because of their prominence. These networks are trained with data taken from the ImageNet database. The filters of the network layers are used to differentiate between input features such as colors, and vertical and horizontal lines. As a consequence of this, it is possible to recognize even little forms and sections. The category to which the input image belongs can be ascertained from the generated output (cats, birds, or other categories, for example). After that, the pre-trained network is used to execute transfer learning by identifying individual records in a new dataset. In this case, the network is used for wrinkle classification. The parameters that were learned during training from the source job were frozen, and then they were sent to the target task. The only exceptions to this rule were the last three layers (FCL, SM, and classification). In addition, the already-trained layers of the pre-trained network are incorporated with these layers to provide a new classification for the classes. As a consequence of this, the training procedure may be finished in a portion of the time using a modest amount of data that is necessary for CNN training to start from scratch. The categorization of wrinkles according to a transfer learning-based technique is shown in Fig. 6.

VGG-16 for feature extraction: At the step of feature extraction, several convolution layers are utilized to identify whether or not specific patterns and features are present in the data that is being processed. There is a total of 13 convolutional layers and three fully connected layers in the VGG-16 architecture [43]. Inside each of these layers, there are three 3×3 kernels and two 2×2 parameters. In this study, the fully linked layers that can be observed in VGG-16 are not used for classification; rather, LSTM is used in its place. The VGG-16 network is structured with convolutional as well as pooling layers divided into 1–5 block groups. Each block includes several convolutional layers as well as a pooling layer. The pooling layer in block 1 uses 16 kernels to extract features for each of the two convolutional layers, hence reducing the size of the images. As a result, the images' overall size is reduced. The design of the subsequent blocks is the same, with the exception that blocks 1 and 2 employ two convolutional layers, whereas blocks 3–5 employ three convolutional layers, each with a distinct kernel number. Both accuracy and network expansion are made possible by this. There are two convolutional layers in Blocks 1 and 2. There are three convolutional layers in blocks 3–5. The breakdown of the VGG-16 model may be found in Fig. 7.

To generate activation maps with dimensions of 240 by 240 by 64, features are collected from input data with dimensions of 240 by 240 by 3 in the initial convolution layer using 64 kernels with dimensions of 3 by 3. The activation maps, which are also referred to as feature maps, appear to be a collection of feature activation recognized by neurons in every convolution layer and have the dimensions of height, breadth, and channel. The succeeding convolution layer took these feature maps as input and sequentially processed them to discover higher-level features. These maps were utilized as input by the layer that came after it. By applying a series of convolution layers in succession, the spatial dimensions of feature maps may be greatly reduced from 240 by 240 to 7 by 7, hence reducing the file size of the feature maps. This indicates that neurons located in deeper convolution layers were the ones to detect the patterns, and they did so depending upon the larger geographical areas of the data. The training was provided to filters in shallow layers so that they could recognize fundamental characteristics, such as colors and edges, that were present in receptive fields. Filters located in the deeper levels were utilized to retrieve the shallower layers. The feature map that is currently in the last convolution layer is first flattened into a single-dimensional vector to do classification. The LSTM model generates output that is divided into two classes namely, wrinkles and non-wrinkles by making use of hidden layers.

2.5 Module 3: detection of stroke

This section describes the prediction of the possibility of stroke using the XGBoost model.

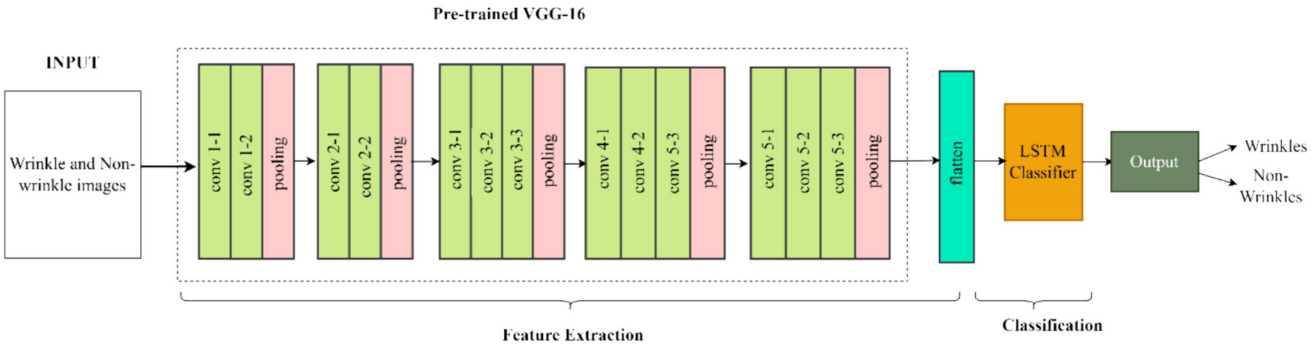


Fig. 6 Classification of Wrinkles using Pre-trained VGG-16 and LSTM

Layer (type)	Output Shape	Param #
input_1 (InputLayer)	[(None, 240, 240, 3)]	0
block1_conv1 (Conv2D)	(None, 240, 240, 64)	1792
block1_conv2 (Conv2D)	(None, 240, 240, 64)	36928
block1_pool (MaxPooling2D)	(None, 120, 120, 64)	0
block2_conv1 (Conv2D)	(None, 120, 120, 128)	73856
block2_conv2 (Conv2D)	(None, 120, 120, 128)	147584
block2_pool (MaxPooling2D)	(None, 60, 60, 128)	0
block3_conv1 (Conv2D)	(None, 60, 60, 256)	295168
block3_conv2 (Conv2D)	(None, 60, 60, 256)	590080
block3_conv3 (Conv2D)	(None, 60, 60, 256)	590080
block3_pool (MaxPooling2D)	(None, 30, 30, 256)	0
block4_conv1 (Conv2D)	(None, 30, 30, 512)	1180160
block4_conv2 (Conv2D)	(None, 30, 30, 512)	2359808
block4_conv3 (Conv2D)	(None, 30, 30, 512)	2359808
block4_pool (MaxPooling2D)	(None, 15, 15, 512)	0
block5_conv1 (Conv2D)	(None, 15, 15, 512)	2359808
block5_conv2 (Conv2D)	(None, 15, 15, 512)	2359808
block5_conv3 (Conv2D)	(None, 15, 15, 512)	2359808
block5_pool (MaxPooling2D)	(None, 7, 7, 512)	0

Fig. 7 Summary of the VGG-16 model

The prediction model for stroke incorporates data from two key models: Model 1 evaluates the presence of Parkinson's disease and overall health status, while Model 2 assesses the presence of wrinkles as a factor. Additionally, various other parameters play a crucial role in this predictive model. These include age, heart disease, gender, marital status, hypertension, employment status, place of residence, average glucose levels, body mass index (BMI), and smoking habits. By integrating information from these diverse sources, the predictive model enhances its accuracy in identifying individuals at risk of stroke. Figure 8 indicates the comprehensive factors in the stroke prediction model.

2.5.1 Dataset

Out of a cohort of 102 patients, a noteworthy observation was made: 24 individuals were found to be afflicted with both wrinkles and Parkinson's disease. It is crucial to highlight that these particular patients played a pivotal role in furnishing the data utilized to construct the dataset featured in this section. The information derived from this subset of patients forms a critical component of the dataset, contributing significantly to the predictive modeling employed in this section, specifically focused on stroke prediction. It has eleven attributes, including gender, age, ID, body mass index (BMI), heart disease, hypertension, ever marriage, kind of employment and habitation, average glucose level, and smoking status, among others. The dataset is split into a training dataset that makes up 80% of the total and a test dataset that makes up the remaining 20%. The training dataset is employed for modeling training and optimization.

2.5.2 Pre-processing

Processing the data appears to be an essential step before the training process, given that the precision of the data has a direct impact on the reliability of the model's predictions. It also involves deleting duplicate values and null values, as well as restoring any data that were previously lost. Deleting duplicates is crucial due to the possibility of patients submitting forms multiple times, causing issues in stroke disease prediction. Removing duplicate entries ensures a high-quality and consistent dataset, preventing noise that can arise from duplicate records and compromise model training accuracy. This action also addresses the risk of overfitting, where the model memorizes training data instead of learning patterns. This promotes better model performance on unseen data and optimizes computational resources during training. Additionally, removing



Fig. 8 Comprehensive Factors in Stroke Prediction Model

duplicates helps avoid biased learning experiences, ensuring a more balanced and unbiased model. The faulty attribute columns that had missing value ratios of more than 70 percent were removed, and mean values were inserted into the remaining feature columns in their stead. Importantly, this process did not result in a decrease in the number of records. Removal of faulty columns and mean imputation preserved the overall dataset size. To make the information more relevant, the data were additionally standardized using the maximum-minimum norm approach. The formula may be written down as follows. The formula is presented in the following way.

$$G = \frac{G^{o} - G^{\min}}{G^{\max} - G^{\min}} \times (\mathrm{NG}_{\max} - \mathrm{NG}_{\min}) + \mathrm{NG}_{\min} \tag{6}$$

where G is the normalized value, Go is the original value, Gmin is the minimum, Gmax is the maximum, and NG max and NG mindenote the series of values that are contained in the updated dataset, with NG max normally equaling 1 and NG min typically equaling 0. The experimental dataset for this study is denoted by the letter G, and its range is between 0 and 1.

2.5.3 SMOTE based data-balancing

In machine learning, data sampling also referred to as balancing is a popular technique for handling uneven data. The three subcategories of over-sampling, under-sampling, and hybrid techniques are further divisions of this methodology. The goal of the under-sampling method is to accomplish the same outcome by removing data values from the category that contains the majority of the items. The strategy of over-sampling brings the data in training up to a more even keel by adding data values for the minority group. On the other hand, the hybrid technique can produce balanced data since it incorporates both over-sampling and under-sampling processes. In this work, a hybrid SMOTE-ENN [44] strategy is utilized to balance the imbalance training datasets for stroke illness. SMOTE was widely used to oversample the minority class to ensure that the dataset would eventually be balanced. Following that, the edited nearest neighbor (ENN) method was applied to maintain balanced distributions while simultaneously decreasing unwelcome sample overlap between two classes. The implementation of SMOTE-ENN results in an increase in the total number of minority classes as well as a more even distribution of the adjusted minority class proportion throughout the dataset. This results in an equal number of classes for strokes and classes without strokes in both categories. The size of the dataset after applying the SMOTE technique is 192.

2.5.4 Deep learning-based possibility of prediction of stroke

It has been described how the machine learning-based XGBoost (Extreme Gradient Boosting) model may detect early strokes by depending on the biomarkers (Parkinson's and wrinkles) that were predicted in earlier parts. The loading of pre-processed data into the model for optimization and training is illustrated in Fig. 9.

Feature selection: It is vital to have a solid understanding of how the model's qualities play a role in prediction to get higher performance from the model. While making a forecast with the XGBoost model, it is essential to take into account the most relevant characteristics. The selection of features is becoming an increasingly crucial

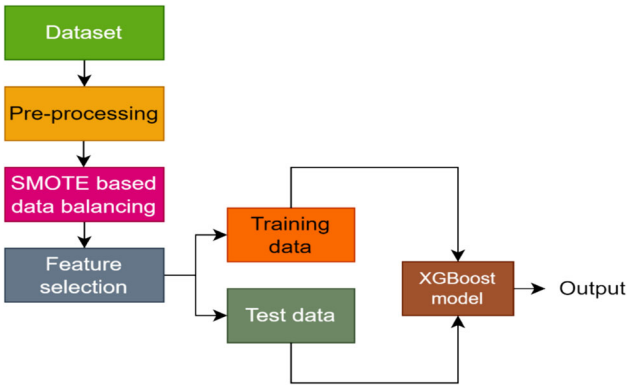


Fig. 9 Stroke disease prediction using XGBoost

process as a data set's number of variables and characteristics grows.

The process of feature selection involves doing an analysis of the datasets as well as selecting the characteristics that, when combined, will supply the vital information that is required to develop the requisite knowledge. This will result in fewer duplicate components while also increasing classification efficiency and precision. Reducing the number of parameters, shortening the training period, eliminating overfitting through increased generalization, and overcoming the dimensionality constraint all contribute to the model's simplification. To make accurate predictions, it is necessary to choose and train on the attributes that have the highest relevance scores.

XGBoost is an improved variation of the generalized additive model (GBM) that is capable of avoiding overfitting and has increased processing efficiency. The operation of XGBoost involves minimizing the impact of several loss functions and using several regularization procedures. The extra regularization period helps to minimize overfitting by providing a smoother experience overall for the final learned weights. Due to its robust handling of a wide range of data types, correlations, and distributions, as well as the vast number of hyperparameters that the user can fine-tune, the XGBoost approach does exceptionally well in machine learning competitions. XGBoost could automatically build gradient tree-boosting strategies in parallel by utilizing a multi-thread processor. This made it possible for the strategies to execute more quickly and improved the accuracy of the method. It is possible to make the forecast by employing the collection of decision trees, and the result is shown as,

$$\hat{z}_i = \sum_{d=1}^{d} f_d(x_i), f_d \in F \tag{7}$$

In the equation presented above, the notation $z\ I$ refers to the ith example sample data included in the training dataset, and the notation x i specifies the anticipated location of the ith instance inside d-th tree. $f_d\,(x_i)$ is the expression that represents the value of the dth tree. The function F is a representation of every value that the decision trees determine. The loss function's parameters must be optimized before starting the model's training process. The following could be used to express it:

$$L = \sum_{i=1}^{n} L(\hat{z}_i, z_i) \tag{8}$$

Although XGBoost appears to be a technique that relies on decision trees, it makes use of a variety of tree-based hyperparameters, such as subsample and max depth. These factors improve prediction accuracy while also reducing the risk of overfitting. In addition to this, the learning rate affects the tree weight of the model, and it may be adjusted to slow down the rate at which the model adjusts to new training data. Because the XGBoost objective function includes a regularization concept, both the process of selecting the prediction function and the management of the complexity of the model are made simpler. The loss function and the regularization term are combined to create the objective function for the XGBoost method. The regularization term governs the model's complexity, and the loss function ascertains the model's level of predictiveness.

The XGBoost's objective function may be stated as follows:

$$\text{Obj} = \sum_{i=1}^{n} L(\hat{z}_i, z_i) \sum_{i=1}^{d} P(f_i) \tag{9}$$

In Eq. (7), the symbol L symbolizes the loss function, which defines the extent to which the model is compatible with the training data; the symbols z I and $z\ i$ show, respectively, the predicted label and the actual label. A penalty is applied based on the complexity of the training tree when employing function P. (f). This also fixes the problem with the item being too large. To determine complexity, a tree function denoted by $f(x)$ has to be defined. As a direct consequence of this, the objective function is expressed as.

$$f(x) = S_{m(x)}, S \in P^N \tag{10}$$

S indicates the leaf scores vector; a mapping function is indicated as m that maps data cases to the respective leaf. Whereas N indicates the number of leaves.

$$P(f) = \gamma D + \alpha(||w||) + \frac{1}{2}\lambda(||w||^2) \tag{11}$$

While and stand for hyperparameters, the whole number of leaves that are included in the tree is represented by the letter D, and this letter can also stand for the complete number of leaves. The L2-norm of the weight of the leaf can be expressed as the notation |(|wl)|2, while the L1-norm

of the weight of the leaf can be represented as the notation |(|wl)|. Regularization at the L1 and L2 levels, which is guided by reg lambda and reg alpha terms, respectively, is responsible for the sparseness that is produced. A minimal loss mitigation is required for the upcoming partition, and this is defined by the hyperparameter c. (gamma).

The utilization of gradient descent resulted in an enhancement to the model's goal function. The model was additive, which means that a tree will be added to the model if the projected outcome matches the total of the trees that are already in the model as well as any new trees that are added. As a consequence of this, the aim at each stage might be stated as, for example, in the twelfth stage (12).

$$\text{Obj}^{(t)} = \sum_{i=1}^{n} L(z_i, \hat{z}_i^{(t-1)} + f_t(x_i)) + P(f_t) + \text{Const} \qquad (12)$$

Because it is difficult to compute all of the potential tree configurations at the same time, the tree structure was developed by first making an estimate of the leaf scores, then applying regularization, and then determining the goal function at each level. Later iterations of this tree structure might be replicated, thereby greatly reducing the computational complexity. In addition, the technique for node splitting is what decides the gain of each feature. It did this continuously up until the maximum debt reached h, at which time it stopped. As a direct consequence of this, the nodes were cut using a declining gain, beginning at the root of the tree. XGBoost locates data and navigates through trees using this method. The eventual output of the model will be the probability that the patient will suffer from stroke illness. This will be of assistance in the early detection of the possibility of a stroke occurring.

2.5.5 Hyperparameter optimization

Hyperparameter optimization refers to the process of selecting the optimal values for a machine learning algorithm's hyperparameter so that the algorithm may get the best possible results when tested on a validation set. Grid, random, and manual methods are all available. Bayesian optimization is one of the most common approaches used in the process of optimizing hyperparameters. Because there are so many hyperfactors, manual search has become more difficult. When it comes to finding hyperparameters, Bayesian optimization is a more comprehensive and time-efficient method. There is no requirement to make any adjustments to any of the hyper settings. In this stage, the primary challenge is the precise selection of parameters from multiple hyperparameters, a task efficiently addressed through hyperparameter tuning [52]. This article employed Bayesian optimization in a systematic four-step process:

Domain Space Initialization: A domain space encompassing a range of values is established, considering input variables such as max depth, reg lambda, cosample bytree, subsample, n estimators, learning rate, regular alpha, min child weight, and gamma.

Objective Function Definition: An objective function is defined, as capable of returning a real number that must decrease to achieve the desired goal. Minimizing the validation error of XGBoost concerning hyperparameters is crucial for accuracy optimization.

Application of Optimization Algorithm: The Bayesian optimization concept is utilized during the tuning phase to construct a surrogate objective function. This method, based on Bayes' theorem, proves efficient in addressing global optimization challenges. The real objective function evaluates candidate samples.

Results Acquisition: Results are scored through value pairs, guiding the algorithm in building the XGBoost model.

This systematic approach ensures efficient hyperparameter tuning, particularly when dealing with complex optimization challenges. Throughout this study, we worked to optimize nine different parameters, including max depth, reg lambda, cosample bytree, subsample, n estimators, learning rate, regular alpha, min child weight, and gamma. Overfitting is prevented by the minimum child weight, gamma, subsample, colsample bytree, and maximum depth parameters, while the learning rate contributes to the robustness and stability of the model. When models get more complex, regularization variables like reg lambda and reg alpha punish them and drive them to become simpler models. These variables are known as "regularization" variables.

3 Result and discussion

3.1 Experimental design

Python, a programming language, is used to implement the recommended models, and the PyTorch module, which is based on machine learning, is used. It would appear that Python is compatible with PyTorch, and it is possible to use Python to construct neural networks. This is beneficial for activities performed by both the CPU and the GPU. To fine-tune the hyperparameters of the model, two methods are used: a network search and the parameters for which the model performs better on the test data that is presented. Choosing the most appropriate values for a model's hyperparameters is an integral part of the training process. The performance review is broken down into three parts: wrinkles, Parkinson's disease, and stroke disease.

3.2 Performance evaluation of Parkinson's disease

During the training of the model, hyperparameters are tweaked to achieve the best possible results from the model. The DenseNet-201 model was optimized with the following hyperparameters: epoch = 50, batch size = 32, optimizer = adam, and activation function = ReLU. These values were chosen since they were determined to be the most effective. The outcomes for the various optimizers are presented in Table 2. The Adam optimizer delivers the best results, followed by the SGD and RMSprop optimizers.

The metrics like precision, accuracy, recall, F1-score, kappa score, MAE, loss, R2, and MSE were used to analyze the outcome of the experiment.

Accuracy: The accuracy is nothing but the percentage of all the pixels in the images that have been accurately labeled, accounting for the entire range of pixel values. It evaluates the correctness of every pixel in the image.

$$\text{Accuracy} = \frac{\text{TP} + \text{TN}}{\text{TP} + \text{TN} + \text{FP} + \text{FN}} \tag{13}$$

The ratio of precisely labeled positive samples to the total number of positive samples identified (accurately or wrongly) can be used to determine the precision. Compared to the standard accuracy measure, the F1-score strongly predicts the classifier's performance.

$$\text{Precision} = \frac{\text{TP}}{\text{TP} + \text{FP}} \tag{14}$$

$$\text{Sensitivity/recall} = \frac{\text{TP}}{\text{FN} + \text{TP}} \tag{15}$$

$$F1 - \text{score} = \frac{2 * \text{ Precision } * \text{ Recall}}{\text{Precision } + \text{ Recall}} \tag{16}$$

Table 3 presents a comparison of the performance of the proposed model to that of several currently used models, including AlexNet, CNN, and SVM. The best possible accuracy was achieved by the proposed DenseNet-201 model, which came in at 93.3%, which is higher than the accuracy achieved by other techniques. In addition, the model that was recommended performs better than other models in terms of recall, kappa score, F1-score, accuracy, MAE, MSE, and R2.

In Figs. 10 and 11, DenseNet-201 outperforms AlexNet, CNN, and SVM across most performance measures, demonstrating superior accuracy, error handling, and predictive capability.

Table 2 Different optimizers for the proposed DenseNet-201 model

Optimizer	Accuracy (%)
Adam	92.12 ↑
SGD	91.54
RMSprop	85.16

Kappa score: It appears that kappa [46] is a statistical measure that represents the degree to which two raters agree with one another. It is a dependable measurement that possesses an easy computation as well as an output range that falls between -1 and 1. The following is the formula used to calculate kappa values:

$$k = \frac{p_0 - p_c}{1 - p_c} \tag{17}$$

The possibility that rankers will agree on everything is denoted by the symbol p 0 in the equation shown above, while the likelihood that they will agree by chance is denoted by the symbol p c. In this situation, the rankers are determined by the real class, also known as the ground truth, as well as the forecasted class, which is created by the classification algorithm. Researchers in [46] discovered that a kappa value of $0 > 75$ showed high agreement, a value of 0.4–0.75 suggested fair to good agreement, and a value of 0.4 indicated poor agreement. This was determined even though there is no one technique to analyze kappa values. Although the possibility of a negative kappa value exists, in reality, this scenario does not come up very often. Kappa is chosen as a performance indication rather than the standard accuracy metric since our datasets are unbalanced for a substantial number of experiments. This is because kappa allows for more room for error. Because of this characteristic, relying on the usual metrics to evaluate the accuracy of categorization might lead to misleading results. The suggested model has a kappa value of 0.594, which is considered to be satisfactory to good and is within the range of 0.4–0.75 points. This reasonable figure was achieved by providing the model with balanced data.

Mean absolute error (MAE), root mean square error (RMSE), and the coefficient of determination R2 were the three statistical assessment metrics that were used to test the success of the prediction strategy [47]. (18) reflects the assessment measures that are related to the Eqs. (20).

$$\text{MAE} = \frac{1}{N}\sum_{j=1}^{N}\left|\widehat{y_j} - y_j\right| \tag{18}$$

$$\text{RMSE} = \sqrt{\frac{\sum_{j=1}^{N}\left(\widehat{y_j} - y_j\right)^2}{N}} \tag{19}$$

$$R^2 = \frac{\sum\left(y_j - y_j\right)^2}{\sum\left(y_j - \overline{y_j}\right)^2} \tag{20}$$

In the above equation, y_j represents the actual value, whereas $\widehat{y_j}$indicates the predicted value by the method, and $\overline{y_j}$ represents the average of $[y_1, y_2, \ldots, y_N]$. Similarly, N indicates the total number of samples.

Table 3 Performance comparison of proposed DenseNet-201 with other models

Parameters	Proposed DenseNet-201	AlexNet [26]	CNN [27]	SVM [50]
Accuracy (%)	93.3 ↑	86.45	84.32%	80.17
F1-score (%)	93.2 ↑	89.9	84.89	83.9
Precision (%)	93.7 ↑	91.0	82.78	81.56
Recall (%)	93.6 ↑	89.1	87.12	86.45
Kappa score	0.594 ↑	0.484	0.362	0.296
MAE	0.02000 ↓	0.077	0.043	0.035
MSE	0.02000 ↓	0.044	0.032	0.028
R^2/R-square	0.949 ↑	0.860	0.894	0.921

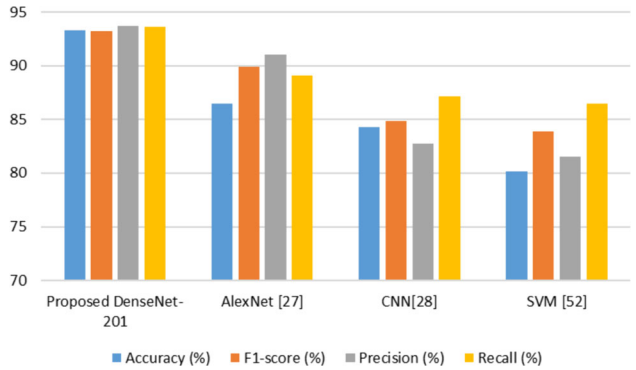


Fig. 10 Comparison of accuracy, precision, F1-score, and recall of various models

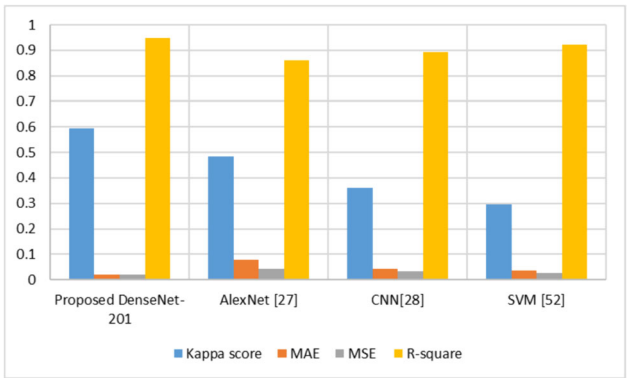


Fig. 11 Comparison of the kappa score, MAE, MSE, and R-square of different models

Training and validation accuracy

Figure 12 depicts the proposed DenseNet-201 models' accuracy training and validation dataset. As compared to the model's training accuracy, the suggested model achieved the best level of validation accuracy. The level of validation accuracy achieved by the model is 93.3% at its peak. It is important to point out that the DenseNet-201 is capable of providing an accurate diagnosis to patients even in the earliest stages of their sickness. This demonstrates

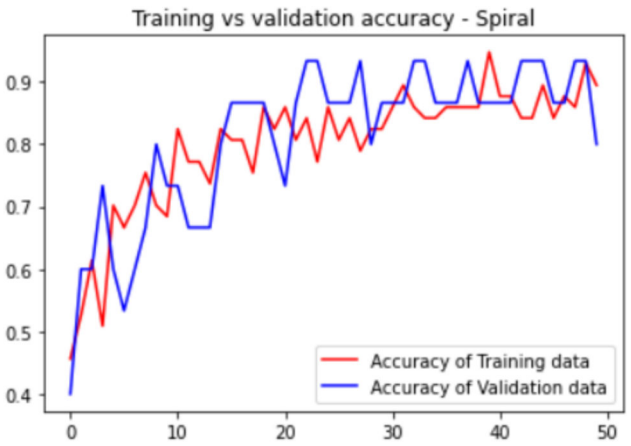


Fig. 12 Training and validation accuracy

that the model has the potential to detect Parkinson's disease earlier, which is a challenge for medical professionals.

Training and validation loss

One of the most significant components of neural networks is the loss function, which establishes the degree of prediction accuracy of a model. Train data were used to educate the model, which was then used to make predictions. Next, for evaluating the deep learning method's performance over the validation set in the classification of unseen images, validation loss has been utilized.

The model loss after implementing the suggested DenseNet-201 model both to training and validation datasets for 50 epochs is shown in Fig. 13. By epoch 50, the model loss has decreased to a reasonably low level in comparison to losses observed in earlier epochs. The training loss and validation losses are found to be the same at epoch 4. This shows that during training and validation, Model 1 suffers a small loss. The DenseNet-201 model came up with a validation loss of 0.2168 when it was used. The spiral photographs are pre-processed to remove any unnecessary information that could have an impact on the accuracy of the forecast before they are introduced into the models. Before the spiral images are given as input to the models,

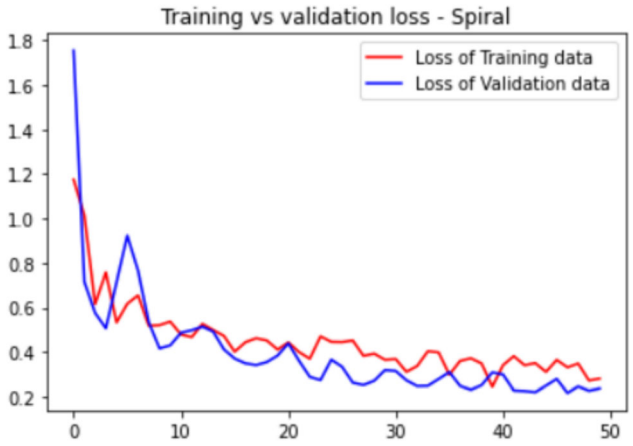


Fig. 13 Training and validation loss

this is completed. Additionally, both models benefit from the Adam optimizer, a complimentary tool that helps them both improve the neural networks during training. Both models experience a steady decrease in training loss throughout the 50 epochs.

3.3 Performance evaluation of wrinkles

Epochs = 150, batch size = 16, optimizer = adam, and activation function = softmax were chosen as the ideal hyperparameters for the hybrid model that was created using VGG-16 and LSTM. The Jaccard similarity index (JSI) is utilized here, in addition to the elements that were discussed in the part that came before this one. Ng et al. [48] investigated the usefulness of their wrinkle detection methods by employing JSI. The intersection of two sets, which is determined by dividing their union, is the Jaccard index between those sets. Two pictures are compared by analyzing their similarities and differences using the Jaccard Index [49].

$$\text{Jaccard index} = \frac{|M \cap N|}{|M \cup N|} \tag{21}$$

In this case, the notation $|M|$ denotes the cardinalities for the set M, whereas $|N|$ denotes the cardinalities for the set N. In this body of work, utilizing the dataset at hand, an investigation of the reliability of wrinkle identification approaches was carried out. The evaluation gave the proposed hybrid model a score of 0.82, indicating that it performed very well. As a result, the model that was recommended had a superior performance in spotting wrinkles when compared to earlier models. When compared to other models that are already in existence, it can be shown that the hybrid model appears to have the lowest MAE and MSE values. This is because the photographs went through a pre-processing step that improved their quality and removed noise from them. The elimination of noise amplification is the primary goal of the CLAHE algorithm. In addition, the hybrid model that is presented in Table 4 has outperformed well in terms of precision, recall, accuracy, F1-score, and kappa score. These other models include CNN + GAN, Resnet-152, and VGG-19.

Figure 14 is a representation of the training accuracy as well as the training loss for the hybrid model that was presented. The training process, as well as the learning process that occurs within the network, are both shown by the training loss curve that was acquired for our model. It is assumed that the loss function will produce the quantitative loss value at the epoch that you choose even if it is computed across every data item throughout an epoch. The hybrid approach that was recommended produced around one hundred percent accuracy in roughly one hundred fifty epochs. This is because of the utilization of data reasoning as well as the process of fine-tuning. Throughout the retraining procedure that lasted for 150 epochs, some model layers were locked in place, while the remaining layers were fine-tuned only by making use of the dataset that was under consideration. This suggests that no alterations were made to any of the image features that were taken from the standard ImageNet dataset before being included in VGG-16. This observation lends credence to the hypothesis that shallow features are more universal than deeper ones. This is because shallow features acquire basic patterns, such as edges, colors, and arcs.

Table 5 highlights the performance comparison between VGG-16 and the proposed VGG-16 with LSTM. The proposed model surpasses VGG-16 in accuracy, precision, and recall, demonstrating its superior ability to identify positive instances and capture relevant cases. Notably, the F1-score further reinforces the proposed model's superiority, with a higher value of 0.96 compared to VGG-16. This emphasizes the overall enhanced performance achieved by integrating LSTM into the VGG-16 architecture, suggesting its effectiveness in improving predictive capabilities for wrinkle detection.

3.4 Performance evaluation of stroke disease

As was previously mentioned, the dataset for the identification of stroke disease is constructed. In this study, each system (Model 1, Model 2, Model 3) is trained independently. To illustrate, let's consider the scenario where the details of User 1 (Patient 1) are inputted into these models. Archimedean spiral images and corresponding face photos of Patient 1 are gathered and simultaneously fed into Model 1 and Model 2. Subsequently, the results from both Model 1 and Model 2 are updated in a.Csv file. This file encompasses various attributes such as gender, age, body mass index (BMI), marital status, occupation category, identification, habitation type, presence of hypertension,

Table 4 Performance comparison of proposed hybrid VGG-16 and LSTM with other models

Parameters	Proposed hybrid model	CNN + GAN [37]	Resnet-152 [34]	VGG-19 [51]
Accuracy	1.000 ↑	0.912	0.926	0.930
F1-score	1.000 ↑	0.908	0.925	0.928
Precision	1.000 ↑	0.909	0.926	0.931
Recall	1.000 ↑	0.910	0.926	0.930
Kappa score	1.000 ↑	0.457	0.672	0.872
MAE	0.000 ↓	0.144	0.108	0.096
MSE	0.000 ↓	0.0518	0.038	0.0251
R^2	1.000 ↑	0.871	0.915	0.943
Jaccard similarity index (JSI)	0.82 ↑	0.61	0.65	0.71

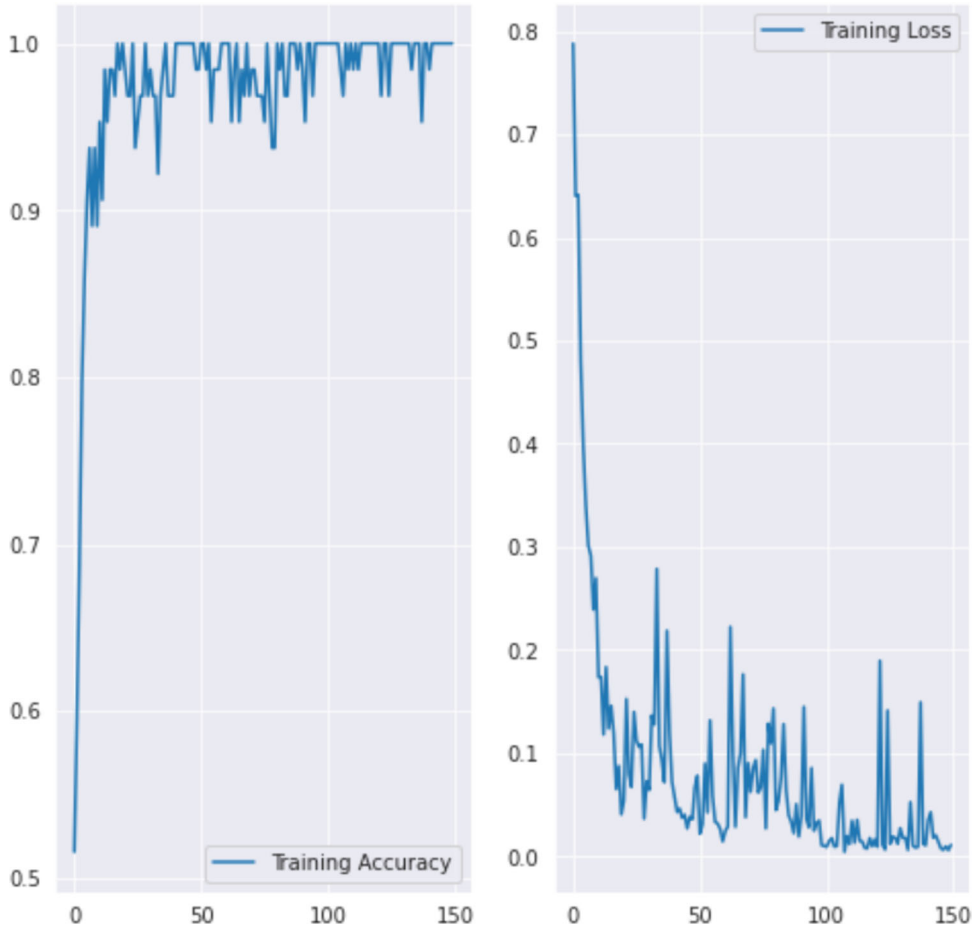


Fig. 14 Training accuracy and loss for epoch = 150

Table 5 Performance comparison of VGG-16 with and without LSTM

Models	Accuracy	Precision	Recall	F1-score
VGG-16 and LSTM (Proposed)	0.95 ↑	0.96 ↑	0.95 ↑	0.96 ↑
VGG-16	0.91	0.93	0.89	0.90

average glucose level, existence of heart disease, and smoking habits. These attributes serve as inputs to an XGBoost model, which predicts the likelihood of stroke disease for Patient 1. The screenshot of.csv file is included

in Fig. 15 in the manuscript containing attributes collected from patients and results of Model 1 and Model 2.

The individuals who belonged to the majority and minority classes in the dataset were categorized as having either the absence (sometimes referred to as the negative class) or the occurrence (also known as the positive class) of stroke illness, respectively. The initial proportion of minority class participants in datasets was 6.55% of all participants (Fig. 16a), and the SMOTE approach has been utilized to enhance the number of minority class samples. To do this, new samples are drawn at random from the samples of the minority class that are included within neural networks using the ENN allowing for the elimination of the overlapping sample sets. The percentage of people who identify as belonging to a minority group has reached 50% as a direct result of the adoption of SMOTE-ENN, which has led to a growth in total diversity and a more equitable society (Fig. 16b).

Figure 17 shows how the attributes in the dataset are related to stroke disease and it is used in the calculation of stroke disease.

The diagnostic form for stroke, which can be seen in Fig. 18a, b and c, allows physicians to fill out patient information, which may include the patient's current circumstances as well as the areas from Fig. 15 that were mentioned. When all of the fields have been filled out, hitting the "submit" button will send the information to the trained recommended XGBoost model, which will then assess the likelihood that the individual is suffering from a stroke ailment. Figure 18c depicts the outcome as it is anticipated to occur.

The dark blue hue stands for a correlation that is close to zero, while the red and orange colors, respectively, depict a correlation that is close to + 1 and also close to 1, respectively. In Fig. 19, the variables residential form and gender have a correlation that is very close to 0. This indicates that both of these factors have a weak or perhaps nonexistent link with the attribute class. As a direct consequence of this, these features are eligible for elimination to make the proposed model more successful. The correlation matrix color map is depicted in Fig. 20, and it reveals that the region in the upper left is highly correlated.

Confusion matrix

A confusion matrix that utilizes the test data is created to assess the efficacy of the proposed model. The rows of the confusion matrix include the data for the actual classes, while the columns contain the data for the predicted classes. This matrix can provide one of four possible outcomes: a true positive (TP), a true negative (TN), a false positive (FP), or a false negative (FN) (FN).

The confusion matrix for the XGBoost model proposed is shown in Fig. 21. It represents the conclusions of an investigation carried out on a dataset for the categories of stroke and no stroke. Eight out of nine cases of stroke illness are diagnosed as strokes, while the ninth case is categorized as not a stroke. The model is accurate in its predictions and reaches a high level of specificity of 89%.

Experiments in this paper use models for identifying stroke illness that make use of random forest, logistic regression, decision tree, Gaussian naive Bayes, support vector machine, XGBoost with hypertuned parameters, and XGBoost. The outcomes of the experiment are shown in terms of accuracy, precision, recall, F1-score, as well as training duration. Based on the criteria of the performance assessment mentioned in Sect. 3.2. (in secs), these metrics have been derived. In the experiments, eighty percent of

1	id	gender	age	hypertensio	heart_dise	ever_mari	work_type	Residence_t	avg_gluco	bmi	smoking_s	stroke	parkinson	wrinkle
2	9046	Male	67	0	1	Yes	Private	Urban	228.69	36.6	formerly s	1	0	1
3	51676	Female	61	0	0	Yes	Self-empl	Rural	202.21		never smc	1	0	0
4	31112	Male	80	0	1	Yes	Private	Rural	105.92	32.5	never smc	1	1	0
5	60182	Female	49	0	0	Yes	Private	Urban	171.23	34.4	smokes	1	0	0
6	1665	Female	79	1	0	Yes	Self-empl	Rural	174.12	24	never smc	1	0	1
7	56669	Male	81	0	0	Yes	Private	Urban	186.21	29	formerly s	1	1	0
8	53882	Male	74	1	1	Yes	Private	Rural	70.09	27.4	never smc	1	0	0
9	10434	Female	69	0	0	No	Private	Urban	94.39	22.8	never smc	1	0	1
10	27419	Female	59	0	0	Yes	Private	Rural	76.15		Unknown	1	1	1
11	60491	Female	78	0	0	Yes	Private	Urban	58.57	24.2	Unknown	1	0	0
12	12109	Female	81	1	0	Yes	Private	Rural	80.43	29.7	never smc	1	0	1
13	12095	Female	61	0	1	Yes	Govt_job	Rural	120.46	36.8	smokes	1	1	0
14	12175	Female	54	0	0	Yes	Private	Urban	104.51	27.3	smokes	1	0	0
15	8213	Male	78	0	1	Yes	Private	Urban	219.84		Unknown	1	1	1
16	5317	Female	79	0	1	Yes	Private	Urban	214.09	28.2	never smc	1	0	0
17	58202	Female	50	1	0	Yes	Self-empl	Rural	167.41	30.9	never smc	1	0	0
18	56112	Male	64	0	1	Yes	Private	Urban	191.61	37.5	smokes	1	1	0
19	34120	Male	75	1	0	Yes	Private	Urban	221.29	25.8	smokes	1	0	1

Fig. 15 Sample screenshot of CSV file

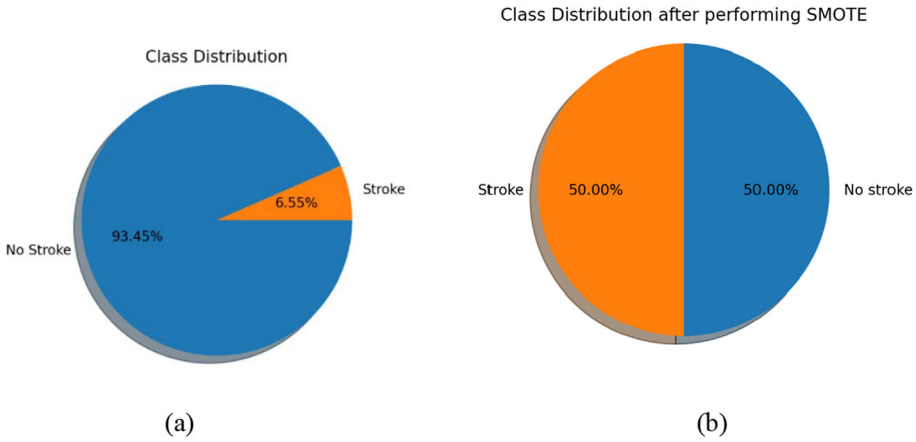


Fig. 16 Class distribution **a** Before SMOTE **b** After performing SMOTE

the total data were used for training, while the remaining twenty percent were used for making predictions and doing the analysis. It has been empirically demonstrated after finishing trials with all of the different deep learning models that the XGBoost model with hypertuned parameters appears to have the maximum projected accuracy at 99.0% while comparing it to other models. This was discovered after completing the trials.

The performance of the recommended model was evaluated further by making use of computing time and contrasting it with a variety of different approaches. The results that were obtained for each of the three approaches in terms of the amount of computational time are presented in Table 6. The new XGBoost architecture proposed only requires 0.36 s of training time, which is a substantial reduction compared to the amount of time needed for training by the various existing techniques. According to the findings, the proposed model is found to be superior in terms of performance to the approaches that are considered to be state-of-the-art.

3.5 Validation of the proposed deep learning models against established medical diagnostics

Proposed deep learning model

The proposed deep learning model leverages noninvasive techniques, utilizing Parkinson's disease and wrinkles as unique biomarkers for early stroke prediction. This approach aims to address the limitations of established medical diagnostics, such as the cost and complexity associated with MRI and CT scans. The model achieves an impressive accuracy of 94.7%, demonstrating its efficacy in predicting strokes at an early stage. The utilization of Archimedean spirals, DenseNet-201, VGG-16, and XGBoost in different stages of the model showcases a comprehensive and innovative methodology.

List of established medical diagnostics for detecting stroke

(I) Clinical Evaluation: physicians perform a thorough clinical assessment, considering symptoms, medical history, and physical examination.

(II) Imaging Tests:

- CT Scan: provides detailed images of the brain to identify bleeding or blockages.
- MRI: utilized for a more comprehensive view of brain structures, useful for detecting ischemic strokes.
- CT Angiography (CTA) and MR Angiography (MRA): visualize blood vessels to identify blockages or abnormalities.

(III) Blood Tests: analyzing blood samples helps identify underlying conditions or risk factors contributing to a stroke.

(iv) Field Triage Stroke Scales: developed for rapid diagnosis and triage, aiding in the swift identification of potential stroke cases in the field.

Comparison of the proposed model with Established Diagnostics

Noninvasiveness: Traditional imaging methods like CT and MRI scans often require invasive procedures. The proposed deep learning model emphasizes noninvasive techniques, offering a less intrusive approach.

Cost and Time Efficiency: CT and MRI scans are known for their high costs and time-consuming nature. The proposed deep learning model is positioned as a cost-effective and time-efficient alternative, potentially reducing financial burdens associated with stroke diagnostics.

Unique Biomarkers: Parkinson's disease and wrinkles serve as novel biomarkers, offering a distinctive approach compared to the generic symptoms considered in established diagnostics.



Fig. 17 Stroke vs attributes

Innovative Methodology: Established Diagnostics follow traditional procedures like CT, MRI, and blood tests. The proposed Model integrates image processing, feature extraction, and machine learning algorithms in a step-wise manner, reflecting an innovative and comprehensive methodology.

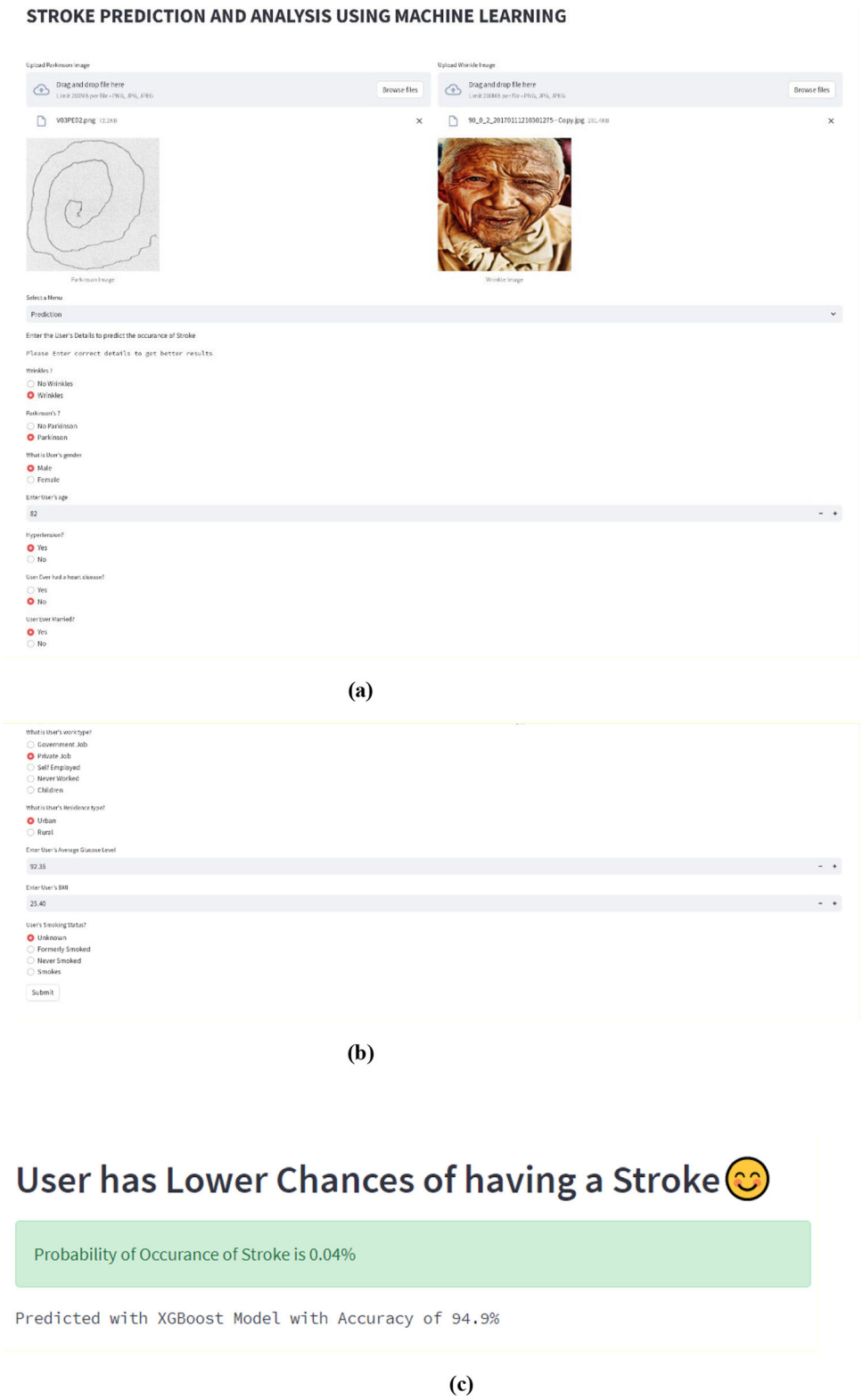


Fig. 18 **a** Diagnosis form collected from patients. **b** Diagnosis form collected from patients. **c** Diagnosis result

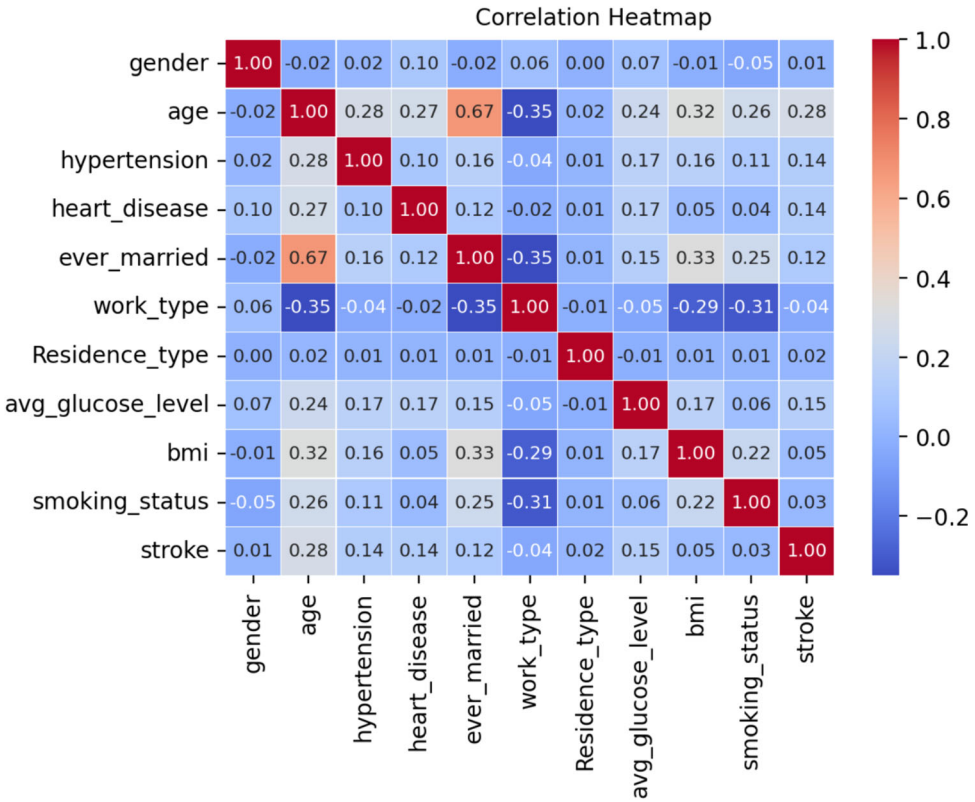


Fig. 19 Heatmap of attributes correlation for a dataset

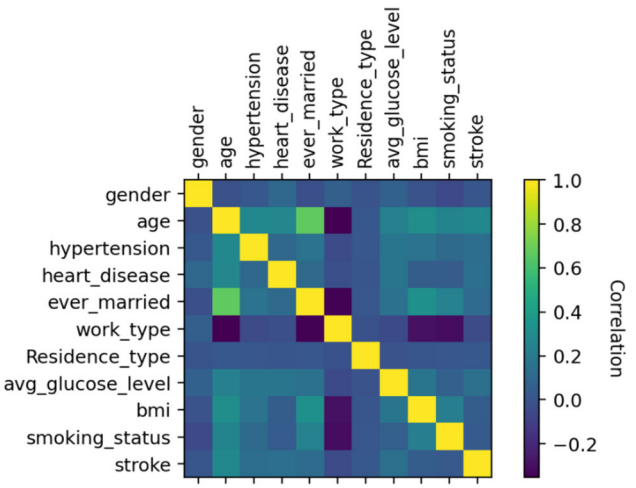


Fig. 20 Correlation matrix color map

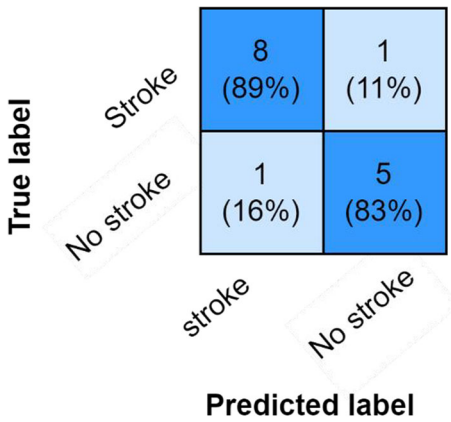


Fig. 21 Shows the Confusion matrix of the XGBoost model proposed

4 Conclusion

A deep learning-based approach to the early detection and diagnosis of stroke illness was presented in this paper. To determine its results, this approach used biomarkers such as wrinkles and Parkinson's disease. If the patient is found to have Parkinson's disease as well as wrinkle disease, then there is a potential that they will have a stroke. Comparing the suggested XGBoost model against other existing models over test data, the assessment of the experiment findings revealed that it had the best stroke prediction accuracy, at 94.9%. By analyzing the models with the test data, this was ascertained. The suggested model outperforms current techniques and yields optimal outcomes in terms of accuracy, precision, recall, F1-score, loss, and training time, according to an analysis of this model against other techniques already in use. The significance of this research lies in its ability to ascertain an individual's risk of stroke before hospitalization. This provides the opportunity to receive treatment within the critical golden time window. Also, this study utilizes a modest dataset for stroke prediction. Future research will be conducted on a more

Table 6 Comparing the Performance of the proposed XGBoost with other models

Models	Accuracy	Precision	Recall	F1-score	Training time (secs)
XGBoost with hypertuned parameters (proposed)	0.99 ↑	0.96 ↑	0.94 ↑	0.95 ↑	0.36 ↓
XGBoost (without hypertuned)	0.94	0.93	0.94	0.94	0.57
Random forest	0.93	0.92	0.93	0.93	0.71
Logistic regression	0.82	0.80	0.84	0.82	1.2
Decision tree	0.89	0.88	0.90	0.89	0.98
Gaussian naïve bayes	0.79	0.75	0.86	0.80	1.45
Support vector machine	0.84	0.83	0.87	0.85	2.87

extensive dataset to improve the robustness and generalizability of predictive models.

Acknowledgements The author would like to appreciate the effort of the editors and reviewers.

Author contributions The author read and approved the final manuscript.

Funding This research received no specific grant from any funding agency in the public, commercial, or not-for-profit sectors.

Data availability All data generated or analyzed during this study are included in the article.

Declarations

Conflict of interest The authors declare that they have no conflicts of interest.

References

1. Choi Y-A, Park S-J, Jun J-A, Pyo C-S, Cho K-H, Lee H-S, Yu J-H (2021) Deep learning-based stroke disease prediction system using real-time biosignals. Sensors (Basel) 21(13):4269. https://doi.org/10.3390/s21134269
2. Lo C-M, Hung P-H (2021) Assessing ischemic stroke with convolutional image features in carotid color Doppler. Ultrasound Med Biol 47(8):2266–2276. https://doi.org/10.1016/j.ultrasmedbio.2021.03.038
3. Kim B, Schweighofer N, Haldar JP, Leahy RM, Winstein CJ (2021) Corticospinal tract microstructure predicts distal arm motor improvements in chronic stroke. J Neurol Phys Ther 45(4):273–281. https://doi.org/10.1097/NPT.0000000000000363
4. Kaur M, Sakhare SR, Wanjale K, Akter F (2022) Early stroke prediction methods for prevention of strokes. Behav Neurol 2022:7725597. https://doi.org/10.1155/2022/7725597
5. Yu J, Park S, Kwon S-H, Cho K-H, Lee H (2022) AI-based stroke disease prediction system using ECG and PPG bio-signals. IEEE Access 10:43623–43638. https://doi.org/10.1109/access.2022.3169284
6. Saba L, Yuan C, Hatsukami TS, Balu N, Qiao Y, DeMarco JK, Saam T, Moody AR, Li D, Matouk CC et al (2018) Carotid artery wall imaging: Perspective and guidelines from the ASNR vessel wall imaging study group and expert consensus recommendations of the American Society of Neuroradiology. AJNR Am J Neuroradiol 39(2):E9–E31. https://doi.org/10.3174/ajnr.a5488
7. Zhou D, Li J, Liu D, Ji L-Y, Wang N-Q, Deng J, Wang J-C, Ye M, Zhao X-H (2019) The irregular surface of carotid atherosclerotic plaque is associated with ischemic stroke: a magnetic resonance imaging study. J Geriatr Cardiol 16(12):872–879. https://doi.org/10.11909/j.issn.1671-5411.2019.12.002
8. Djamal EC, Ramadhan RI, Mandasari MI, Djajasasmita D (2020) Identification of post-stroke EEG signal using wavelet and convolutional neural networks. Bull Electr Eng Inform. 9(5):1890–1898. https://doi.org/10.11591/eei.v9i5.2005
9. Acharya UR, Oh SL, Hagiwara Y, Tan JH, Adeli H, Subha DP (2018) Automated EEG-based screening of depression using deep convolutional neural network. Comput Methods Programs Biomed 161:103–113. https://doi.org/10.1016/j.cmpb.2018.04.012
10. Chambon S, Thorey V, Arnal PJ, Mignot E, Gramfort A (2019) DOSED: A deep learning approach to detect multiple sleep micro-events in EEG signal. J Neurosci Methods 321:64–78. https://doi.org/10.1016/j.jneumeth.2019.03.017
11 Kwon Y-H, Shin S-B, Kim S-D (2018) Electroencephalography-based fusion two-dimensional (2D)-convolution neural networks (CNN) model for emotion recognition system. Sensors (Basel). https://doi.org/10.3390/s18051383
12. Fares A, Zhong S-H, Jiang J (2019) EEG-based image classification via a region-level stacked bi-directional deep learning framework. BMC Med Inform Decis Mak 19(Suppl 6):268. https://doi.org/10.1186/s12911-019-0967-9
13. Kamtchum-Tatuene J, Jickling GC (2019) Blood biomarkers for stroke diagnosis and management. Neuromolecular Med 21(4):344–368. https://doi.org/10.1007/s12017-019-08530-0
14. Chen N-H, Zhang Y-M, Jiang F-P, Liu S, Zhao H-D, Hou J-K, Jiang T, Shi J-Q, Zhou J-S, Zhang Y-D (2022) FLAIR vascular hyperintensity predicts early neurological deterioration in patients with acute ischemic stroke receiving endovascular thrombectomy. Neurol Sci 43(6):3747–3757. https://doi.org/10.1007/s10072-021-05853-4
15. Huo X, Sun D, Raynald JB, Tong X, Wang A, Ma N, Gao F, Mo D, Ma G et al (2022) Endovascular treatment in Acute Ischemic Stroke with large vessel occlusion according to different stroke subtypes: data from ANGEL-ACT registry. Neurol Ther 11(1):151–165. https://doi.org/10.1007/s40120-021-00301-z
16. Zhu H, Jiang L, Zhang H, Luo L, Yang C, Yuchen C (2021) An automatic machine learning approach for ischemic stroke onset time identification based on DWI and FLAIR imaging. NeuroImage Clin 31(102744):102744. https://doi.org/10.1016/j.nicl.2021.102744

17. Vupputuri A, Gupta A, Ghosh N (2021) MCA-DN: Multi-path convolution leveraged attention deep network for salvageable tissue detection in ischemic stroke from multi-parametric MRI. Comput Biol Med 136(104724):104724. https://doi.org/10.1016/j.compbiomed.2021.104724
18. Kauw F, Greving JP, Takx RAP, de Jong HWAM, Schonewille WJ, Vos JA, Wermer MJH, van Walderveen MAA, Kappelle LJ, Velthuis BK et al (2021) Prediction of long-term recurrent ischemic stroke: the added value of non-contrast CT, CT perfusion, and CT angiography. Neuroradiology 63(4):483–490. https://doi.org/10.1007/s00234-020-02526-5
19. Pinto A, Amorim J, Hakim A, Alves V, Reyes M, Silva CA (2021) Prediction of stroke lesion at 90-day follow-up by fusing raw DSC-MRI with parametric maps using deep learning. IEEE Access 9:26260–26270. https://doi.org/10.1109/access.2021.3058297
20. Raghunath S, Pfeifer JM, Ulloa-Cerna AE, Nemani A, Carbonati T, Jing L, vanMaanen DP, Hartzel DN, Ruhl JA, Lagerman BF et al (2021) Deep neural networks can predict new-onset atrial fibrillation from the 12-lead ECG and help identify those at risk of atrial fibrillation-related stroke. Circulation 143(13):1287–1298. https://doi.org/10.1161/CIRCULATIONAHA.120.047829
21. Han C, Kwon O, Chang M, Joo S, Lee Y, Lee JS, Hong JM, Lee S-J, Yoon D (2022) Evaluating the risk of paroxysmal atrial fibrillation in noncardioembolic ischemic stroke using artificial intelligence-enabled ECG algorithm. Front Cardiovasc Med 9:865852. https://doi.org/10.3389/fcvm.2022.865852
22. Xie Y, Yang H, Yuan X, He Q, Zhang R, Zhu Q, Chu Z, Yang C, Qin P, Yan C (2021) Stroke prediction from electrocardiograms by deep neural network. Multimed Tools Appl 80(11):17291–17297. https://doi.org/10.1007/s11042-020-10043-z
23. Noncommunicable diseases. Who.int. [accessed 2023 Aug 2]. https://www.who.int/news-room/fact-sheets/detail/noncommunicable-diseases
24. Maida CD, Daidone M, Pacinella G, Norrito RL, Pinto A, Tuttolomondo A (2022) Diabetes and ischemic stroke: an old and new relationship an overview of the close interaction between these diseases. Int J Mol Sci 23(4):2397. https://doi.org/10.3390/ijms23042397
25. Moetesum M, Siddiqi I, Vincent N, Cloppet F (2019) Assessing visual attributes of handwriting for prediction of neurological disorders—a case study on Parkinson's disease. Pattern Recognit Lett 121:19–27. https://doi.org/10.1016/j.patrec.2018.04.008
26. Cantürk İ (2021) Fuzzy recurrence plot-based analysis of dynamic and static spiral tests of Parkinson's disease patients. Neural Comput Appl 33(1):349–360. https://doi.org/10.1007/s00521-020-05014-2
27. Diaz M, Ferrer MA, Impedovo D, Pirlo G, Vessio G (2019) Dynamically enhanced static handwriting representation for Parkinson's disease detection. Pattern Recognit Lett 128:204–210. https://doi.org/10.1016/j.patrec.2019.08.018
28. Vasquez-Correa JC, Arias-Vergara T, Orozco-Arroyave JR, Eskofier B, Klucken J, Noth E (2019) Multimodal assessment of Parkinson's disease: a deep learning approach. IEEE J Biomed Health Inform 23(4):1618–1630. https://doi.org/10.1109/JBHI.2018.2866873
29. Naseer A, Rani M, Naz S, Razzak MI, Imran M, Xu G (2020) Refining Parkinson's neurological disorder identification through deep transfer learning. Neural Comput Appl 32(3):839–854. https://doi.org/10.1007/s00521-019-04069-0
30. Pereira CR, Pereira DR, Rosa GH, Albuquerque VHC, Weber SAT, Hook C, Papa JP (2018) Handwritten dynamics assessment through convolutional neural networks: an application to Parkinson's disease identification. Artif Intell Med 87:67–77. https://doi.org/10.1016/j.artmed.2018.04.001
31. Rios-Urrego CD, Vásquez-Correa JC, Vargas-Bonilla JF, Nöth E, Lopera F, Orozco-Arroyave JR (2019) Analysis and evaluation of handwriting in patients with Parkinson's disease using kinematic, geometrical, and non-linear features. Comput Methods Programs Biomed 173:43–52. https://doi.org/10.1016/j.cmpb.2019.03.005
32. Impedovo D, Pirlo G (2019) Dynamic handwriting analysis for the assessment of neurodegenerative diseases: a pattern recognition perspective. IEEE Rev Biomed Eng 12:209–220. https://doi.org/10.1109/RBME.2018.2840679
33. Elbashir RM, Hoon YM (2020) Evaluation of automatic facial wrinkle detection algorithms. J Imaging 6(4):17. https://doi.org/10.3390/jimaging6040017
34. Chang T-R, Tsai M-Y (2022) Classifying conditions of speckle and wrinkle on the human face: a deep learning approach. Electronics (Basel) 11(21):3623. https://doi.org/10.3390/electronics11213623
35. Ng C-C, Yap MH, Cheng Y-T, Hsu G-S (2018) Hybrid ageing patterns for face age estimation. Image Vis Comput 69:92–102. https://doi.org/10.1016/j.imavis.2017.08.005
36. Yap MH, Batool N, Ng C-C, Rogers M, Walker K (2021) A survey on facial wrinkles detection and inpainting: datasets, methods, and challenges. IEEE Trans Emerg Top Comput Intell 5(4):505–519. https://doi.org/10.1109/tetci.2021.3075723
37. Kim E-S, Heo J-M, Eun S-J, Lee JY (2022) Development of early-stage stroke diagnosis system for the elderly neurogenic bladder prevention. Int Neurourol J 26(Suppl 1):S76-82. https://doi.org/10.5213/inj.2244030.015
38. Umeda-Kameyama Y, Kameyama M, Tanaka T, Son B-K, Kojima T, Fukasawa M, Iizuka T, Ogawa S, Iijima K, Akishita M (2021) Screening of Alzheimer's disease by facial complexion using artificial intelligence. Aging (Albany NY). 13(2):1765–1772. https://doi.org/10.18632/aging.202545
39 Choudhary K, DeCost B, Chen C, Jain A, Tavazza F, Cohn R, Park CW, Choudhary A, Agrawal A, Billinge SJL et al (2022) Recent advances and applications of deep learning methods in materials science. Npj Comput Mater. https://doi.org/10.1038/s41524-022-00734-6
40. Zhang Y-D, Pan C, Chen X, Wang F (2018) Abnormal breast identification by a nine-layer convolutional neural network with parametric rectified linear unit and rank-based stochastic pooling. J Comput Sci 27:57–68. https://doi.org/10.1016/j.jocs.2018.05.005
41. Saleh K, Hossny M, Nahavandi S (2020) Spatio-temporal DenseNet for real-time intent prediction of pedestrians in urban traffic environments. Neurocomputing 386:317–324. https://doi.org/10.1016/j.neucom.2019.12.091
42. Heo W-H, Kim H, Kwon O-W (2020) Source separation using dilated time-frequency DenseNet for music identification in broadcast contents. Appl Sci (Basel) 10(5):1727. https://doi.org/10.3390/app10051727
43. Jiang Z-P, Liu Y-Y, Shao Z-E, Huang K-W (2021) An improved VGG16 model for pneumonia image classification. Appl Sci (Basel) 11(23):11185. https://doi.org/10.3390/app112311185
44. Fitriyani NL, Syafrudin M, Alfian G, Rhee J (2020) HDPM: an effective heart disease prediction model for a clinical decision support system. IEEE Access 8:133034–133050. https://doi.org/10.1109/access.2020.3010511
45. Wasesa M, Andariesta DT, Afrianto MA, Haq IN, Pradipta J, Siallagan M, Leksono E, Iskandar BP, Putro US (2022) Predicting electricity consumption in microgrid-based educational buildings using Google trends, Google mobility, and COVID-19 data in the context of the COVID-19 pandemic. IEEE Access 10:32255–32270. https://doi.org/10.1109/access.2022.3161654

46. Alissa M, Lones MA, Cosgrove J, Alty JE, Jamieson S, Smith SL, Vallejo M (2022) Parkinson's disease diagnosis using convolutional neural networks and figure-copying tasks. Neural Comput Appl 34(2):1433–1453. https://doi.org/10.1007/s00521-021-06469-7
47. Shahid AH, Singh MP (2020) A deep learning approach for prediction of Parkinson's disease progression. Biomed Eng Lett 10(2):227–239. https://doi.org/10.1007/s13534-020-00156-7
48. Ng C-C, Yap MH, Costen N, Li B (2015) Wrinkle detection using hessian line tracking. IEEE Access 3:1079–1088. https://doi.org/10.1109/access.2015.2455871
49. Saladi S, Karuna Y, Koppu S, Reddy GR, Mohan S, Mallik S, Qin H (2023) Segmentation and analysis emphasizing neonatal MRI brain images using machine learning techniques. Mathematics 11(2):285. https://doi.org/10.3390/math11020285
50. Drotár P, Mekyska J, Rektorová I, Masarová L, Smékal Z, Faundez-Zanuy M (2016) Evaluation of handwriting kinematics and pressure for differential diagnosis of Parkinson's disease. Artif Intell Med 67:39–46. https://doi.org/10.1016/j.artmed.2016.01.004
51. Xiao J, Wang J, Cao S, Li B (2020) Application of a novel and improved VGG-19 network in the detection of workers wearing masks. J Phys Conf Ser 1518(1):012041. https://doi.org/10.1088/1742-6596/1518/1/012041
52. Dalal S, Onyema EM, Malik A (2022) Hybrid XGBoost model with hyperparameter tuning for prediction of liver disease with better accuracy. World J Gastroenterol: WJG 28(46):6551–6563. https://doi.org/10.3748/wjg.v28.i46.6551
53. Liu Y, Xue L, Zhang Y, Xie A (2020) Association between stroke and Parkinson's disease: a Meta-analysis. J Mol Neurosci 70:1169–1176. https://doi.org/10.1007/s12031-020-01524-9
54. Elfil M, Bayoumi A, Sayed A, Aladawi M, Aboutaleb PE, Grieb L, Tolba H, Tinaz S (2023) Stroke in Parkinson's disease: a review of epidemiological studies and potential pathophysiological mechanisms. Acta Neurol Belg 123(3):773–783. https://doi.org/10.1007/s13760-023-02202-4

Publisher's Note Springer Nature remains neutral with regard to jurisdictional claims in published maps and institutional affiliations.

Springer Nature or its licensor (e.g. a society or other partner) holds exclusive rights to this article under a publishing agreement with the author(s) or other rightsholder(s); author self-archiving of the accepted manuscript version of this article is solely governed by the terms of such publishing agreement and applicable law.